Upper Plate and Subduction Interface Deformation Models in the 2022 Revision of the Aotearoa New Zealand National Seismic Hazard Model

Russ J. Van Dissen*[1], Kaj M. Johnson[2], Hannu Seebeck[1], Laura M. Wallace[1], Chris Rollins[1], Jeremy Maurer[3], Matthew C. Gerstenberger[1], Charles A. Williams[1], Ian J. Hamling[1], Andrew Howell[1], and Christopher J. DiCaprio[1]

ABSTRACT

As part of the 2022 revision of the Aotearoa New Zealand National Seismic Hazard Model (NZ NSHM 2022), deformation models were constructed for the upper plate faults and subduction interfaces that impact ground-shaking hazard in New Zealand. These models provide the locations, geometries, and slip rates of the earthquake-producing faults in the NZ NSHM 2022. For upper plate faults, two deformation models were developed: a geologic model derived directly from the fault geometries and geologic slip rates in the NZ Community Fault Model version 1.0 (NZ CFM v.1.0); and a geodetic model that uses the same faults and fault geometries and derives fault slip-deficit rates by inverting geodetic strain rates for back slip on those specified faults. The two upper plate deformation models have similar total moment rates, but the geodetic model has higher slip rates on low-slip-rate faults, and the geologic model has higher slip rates on higher-slip-rate faults. Two deformation models are developed for the Hikurangi–Kermadec subduction interface. The Hikurangi–Kermadec geometry is a linear blend of the previously published interface models. Slip-deficit rates on the Hikurangi portion of the deformation model are updated from the previously published block models, and two end member models are developed to represent the alternate hypotheses that the interface is either frictionally locked or creeping at the trench. The locking state in the Kermadec portion is less well constrained, and a single slip-deficit rate model is developed based on plate convergence rate and coupling considerations. This single Kermadec realization is blended with each of the two Hikurangi slip-deficit rate models to yield two overall Hikurangi–Kermadec deformation models. The Puysegur subduction interface deformation model is based on geometry taken directly from the NZ CFM v.1.0, and a slip-deficit rate derived from published geodetic plate convergence rate and interface coupling estimates.

KEY POINTS

- Deformation models for upper plate faults and subduction interfaces are developed for the New Zealand National Seismic Hazard Model (NZ NSHM) 2022.
- The upper plate geologic-based and geodetic-based deformation models have nearly identical moment rates.
- Upper plate and interface deformation models have been successfully implemented in inversion-based hazard modeling.

Supplemental Material

1. GNS Science|Te Pū Ao, Lower Hutt, New Zealand, https://orcid.org/0000-0001-8224-7573 (RJVD); https://orcid.org/0000-0002-1749-6626 (HS); https://orcid.org/0000-0002-5291-6956 (CR); https://orcid.org/0000-0002-0392-7114 (MCG); https://orcid.org/0000-0001-7435-9196 (CAW); https://orcid.org/0000-0003-4324-274X (IJH); https://orcid.org/0009-0000-5823-0384 (CJD); 2. Department of Earth and Atmospheric Sciences, Indiana University, Bloomington, Indiana, U.S.A., https://orcid.org/0000-0003-1511-5241 (KMJ); 3. Departments of Geosciences and Geological and Petroleum Engineering, University of Missouri Science and Technology, Rolla, Missouri, U.S.A., https://orcid.org/0000-0002-3624-5961 (JM)

*Corresponding author: r.vandissen@gns.cri.nz

Cite this article as Van Dissen, R. J., K. M. Johnson, H. Seebeck, L. M. Wallace, C. Rollins, J. Maurer, M. C. Gerstenberger, C. A. Williams, I. J. Hamling, A. Howell, *et al.* (2023). Upper Plate and Subduction Interface Deformation Models in the 2022 Revision of the Aotearoa New Zealand National Seismic Hazard Model, *Bull. Seismol. Soc. Am.* **114**, 37–56, doi: 10.1785/0120230118

INTRODUCTION

The 2022 revision of New Zealand National Seismic Hazard Model–Te Tauira Matapae Pūmate Rū i Aotearoa (NZ NSHM 2022) provides a comprehensive update of the nation's seismic hazard outlook (Gerstenberger, Bora, *et al.*, 2022; M. C. Gerstenberger *et al.*, unpublished manuscript, 2023, see Data and Resources)—the first in over a decade. This revision entailed significant updates of the component seismicity rate model (SRM; Gerstenberger, Van Dissen, *et al.*, 2022; M. C. Gerstenberger *et al.*, unpublished manuscript, 2023, see Data and Resources) and ground-motion characterization model (Bradley *et al.*, 2022; B. A. Bradley *et al.*, unpublished manuscript, 2023, see Data and Resources). Within the SRM, foundational datasets were compiled and brought up to date, including the historical earthquake catalog (Christophersen *et al.*, 2022; A. Christophersen *et al.*, unpublished manuscript, 2023, see Data and Resources; Rollins *et al.*, 2022; C. Rollins *et al.*, unpublished manuscript, 2023, see Data and Resources) and paleoearthquake timings and recurrence interval datasets (Litchfield *et al.*, 2022, 2023; Coffey *et al.*, 2022, 2023). Constituent models were also either revised and/or developed including the upper plate distributed seismicity model (Rastin *et al.*, 2022; S. J. Rastin *et al.*, unpublished manuscript, 2023, see Data and Resources; Iturrieta *et al.*, 2022; P. Iturrieta *et al.*, unpublished manuscript, 2023, see Data and Resources) and the intraslab seismicity model (Thingbaijam *et al.*, 2022, 2023).

Perhaps the foremost development within the SRM was the adoption of the inversion-based methodology of the Uniform California Earthquake Rupture Forecast, Version 3 (UCERF3; e.g., Field *et al.*, 2014) to derive earthquake rupture rates for major seismogenic faults. This choice necessitated the development of deformation models for the upper plate faults, and subduction interfaces in and around New Zealand. This article focuses on the development of those deformation models.

Following the UCERF3 workflow, and the more recent 2023 U.S. National Seismic Hazard Model (e.g., Hatem *et al.*, 2022; Pollitz *et al.*, 2022), deformation models provide the locations, geometries, and slip rates of the earthquake-producing faults explicitly modeled within the SRM. Deformation models are, in essence, an attempt to distil the seismotectonics of a region into a form that is digestible by the specific hazard engine(s), for example, OpenSHA (Field *et al.*, 2003), OpenQuake (Silva *et al.*, 2014), which are used to derive the earthquake rupture rate and/or ground-shaking hazard estimates.

New Zealand is home to hundreds of mapped upper plate faults, and to the Hikurangi–Kermadec and Puysegur subduction interfaces, and the NZ NSHM 2022 includes deformation models for each of these regimes. The upper plate deformation models consist of a geologic deformation model for which fault slip rates are based on geologic data and inferences, and a geodetic deformation model for which fault slip-deficit rates (i.e., the difference between the long-term slip rate on the fault and the present-day creep rate) are derived from geodetic data and modeling. Of the subduction interface deformation models, two have been developed for the Hikurangi–Kermadec interface (comprising different assumptions about near-trench locking), and one for the Puysegur interface.

A summary of the deformation models developed for the NZ NSHM 2022 is presented subsequently, along with comparisons between the models of, primarily, fault slip rates and moment release rates. Additional detail and supporting information can be found in Van Dissen *et al.* (2022) for the upper plate geologic and subduction interface deformation models, and in Johnson *et al.* (2022) and K. M. Johnson *et al.*, (unpublished manuscript, 2023 see Data and Resources) for the upper plate geodetic deformation model.

UPPER PLATE DEFORMATION MODELS

Geologic deformation model

The geometries and slip rates of the faults and fault sections that comprise the NZ NSHM 2022 geologic deformation model are taken directly from the New Zealand Community Fault Model version 1.0 (NZ CFM v.1.0; Seebeck *et al.*, 2022, 2023; Figs. 1, 2) with the following modifications:

1. There are 159 faults in the NZ CFM v.1.0 that have an unspecified slip rate (Fig. 2a) (denoted as 0 mm/yr in the NZ CFM v.1.0 attribute table), and these are excluded from the geologic deformation model. Most of these faults are offshore or in the remote Southern Alps region of the South Island.
2. There are 53 faults in the NZ CFM v.1.0 with a fault status of A-US (A-US, "active but unlikely to be seismogenic"; Fig. 2b), and these are excluded from the geologic deformation model. Thirty-seven of these also have an unspecified slip rate. A-US faults comprise bedding plane (flexural slip) faults, shallow-seated back thrusts, and shallow-seated forearc thrusts. The vast majority (>90%) of A-US faults are located in the eastern (trenchward) portion of the Hikurangi accretionary margin. These faults propagate through unconsolidated strata and are considered unlikely to generate large earthquakes. Such faults may not pose a ground-shaking hazard but may undergo displacement relevant to tsunami hazard.
3. Of the 212 faults within the Taupō rift–Havre trough region in the NZ CFM v.1.0, the 166 that have slip rates less than 1.8 mm/yr are excluded from the geologic deformation model (Fig. 3). The Taupō rift–Havre trough region is the most densely faulted region in New Zealand, with cross-strike fault spacing in the central part of the rift averaging less than a few hundred meters. With such a high density of faulting, and with commensurate uncertainty regarding how such closely spaced faults may (or may not) coalesce into potential earthquake sources, it was decided that this region would be largely characterized through the distributed seismicity model of NZ NSHM 2022 which, itself, enfolds fault location and slip rate

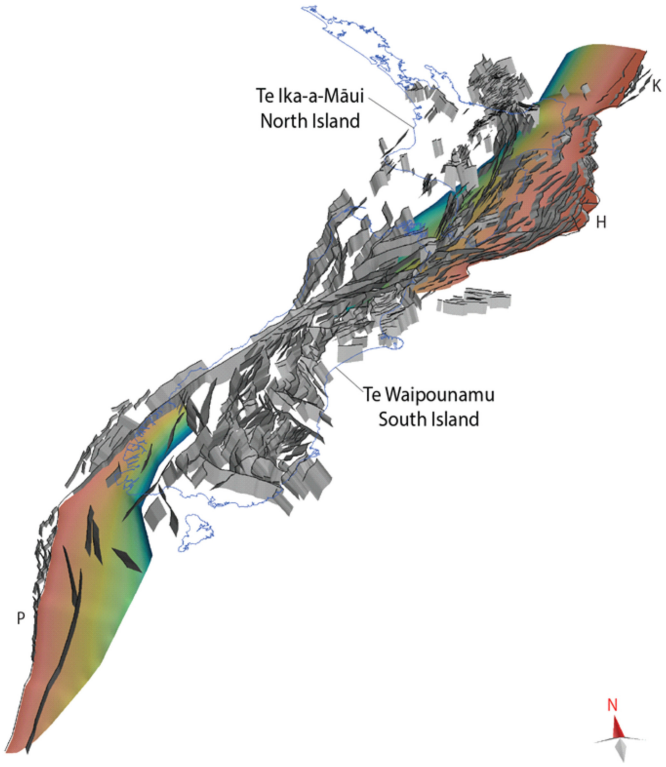

Figure 1. New Zealand Community Fault Model version 1.0 (NZ CFM v.1.0; after Seebeck *et al.*, 2022, 2023). A 3D view looking toward the north showing active and potentially active fault zones along the New Zealand plate boundary represented in the model. The subduction interfaces have been colored according to depth from warm (shallow) to cool (deep) colors to distinguish them from the upper plate fault zones shown in gray. Fault-zone traces at the surface are shown by black lines along with the coastline in blue. H and K denote, respectively, the Hikurangi and Kermadec portions of the Hikurangi-Kermadec subduction interface, and P denotes the Puysegur subduction interface. The fault model has a length, measured along a northeast trend, of ~2100 km, and a width of ~550 km. The color version of this figure is available only in the electronic edition.

(Rastin *et al.*, 2022; S. J. Rastin *et al.*, unpublished manuscript, 2023, see Data and Resources). However, it was considered appropriate to explicitly include the major rift-bounding faults such as the Paeroa fault (Fig. 4) and to have at least one explicitly modeled fault present along most of the length of the rift. A slip-rate filter of ≥1.8 mm/yr satisfied these two criteria (Fig. 3).

NZ CFM v.1.0 lists the maximum fault rupture depths (termed "Dfc") for the fault zones and fault sections in the model. These depths are largely based on seismological and thermal constraints on the down-dip limit of seismogenesis (Ellis *et al.*, 2021, 2023) or the projected depth at which faults would truncate against a more dominant structure, such as the Hikurangi subduction interface or the Alpine fault. Dfc includes a fault rupture "overshoot" factor of 1.25 that accounts for the possibility that large earthquakes may dynamically rupture deeper than recorded seismicity (Ellis *et al.*, 2021, 2023; Seebeck *et al.*, 2022). However, slip in an earthquake probably tapers gradually to zero as it approaches Dfc or its greatest depth (Ellis *et al.*, 2021), whereas a uniform or "boxcar" down-dip slip distribution for coseismic slip on upper plate faults is used in the NZ NSHM 2022. The appropriate bottom depth for this boxcar distribution is not the maximum depth that tapering slip could reach (Dfc) but the depth that allows the lower edge of the boxcar to best approximate the effect of the taper (in terms of total area under the curve), that is, the lower edge of the boxcar will be short of Dfc. Therefore, a fault rupture depth of 0.8 Dfc was assigned for faults outside of the Taupō rift–Havre trough region (basically, the "overshoot" factor was removed). For faults within the Taupō rift, for which heat flow is relatively high and the crust is relatively thin, a fault depth of 0.66 Dfc was assigned.

Figure 5 presents a depiction of the NZ NSHM 2022 geological deformation model, and a csv file of the model is available in supplemental material to this article.

Geodetic deformation model

To incorporate geodetic measurements of contemporary deformation into the NZ NSHM 2022, strain rate and fault slip-deficit rate models are developed utilizing New Zealand's interseismic Global Navigation Satellite Systems (GNSS)-derived velocity field. This work is detailed in Johnson *et al.* (2022), K. M. Johnson *et al.* (unpublished manuscript, 2023) and J. Maurer *et al.* (unpublished manuscript, 2023, see Data and Resources); here, a summary is provided.

Geodetic strain-rate field. The strain rate models are derived from the most current, published, Global Positioning System (GPS) velocity field of New Zealand—that of Beavan *et al.* (2016; Fig. 6), which is based on data acquired between 1995 and 2013, and includes corrections for coseismic offsets of earthquakes during that period. Because the strain rate models are intended to represent strain accumulation on upper plate faults (so that they can be used to derive slip-deficit rates on those faults), two other features of the GPS velocity field were removed: suspected sill cooling in the Taupō volcanic zone (e.g., Hamling *et al.*, 2015; Hamling, Kilgour, *et al.*, 2022) and coupling on the Hikurangi subduction interface (e.g., Wallace *et al.*, 2012). Details of this removal (i.e., adjustment) process are provided in Johnson *et al.* (2022).

From the amended velocity field, strain rate maps are computed using two purely statistical methods and two elasticity-based methods. The first statistical method is VELMAP (Wang and Wright, 2012; Weiss *et al.*, 2020), which solves for a spatially smooth velocity field through traditional second-order Tikhonov regularization. The second statistical method uses geostatistical methods of variogram analysis and kriging to build realizations of the velocity and strain-rate fields with covariance structure inherent to the observed velocities. The two physics-based methods solve for a distribution of body

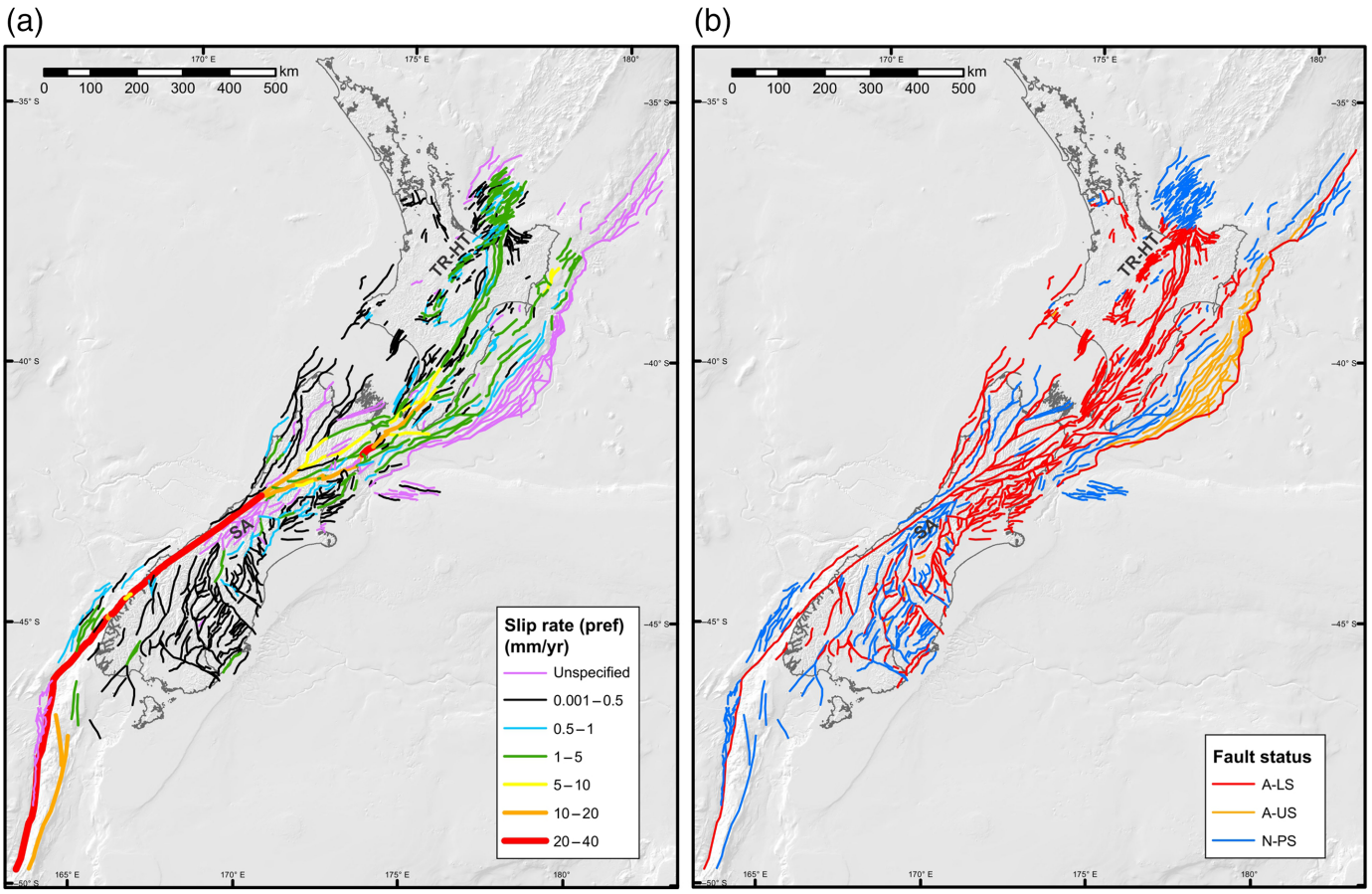

Figure 2. Faults and fault sections in the NZ CFM v.1.0 color coded by: (a) slip rate (preferred) and (b) fault status with A-LS, active and likely to be seismogenic; A-US, active but unlikely to be seismogenic; N-PS, not proven active but considered potentially capable of being seismogenic; SA, southern Alps; TR-HT, Taupō rift–Havre trough. The color version of this figure is available only in the electronic edition.

forces in an elastic plate that explain the observed velocity field and then compute the strain-rate field from the estimated distribution of forces. The vertical derivatives of horizontal stress method uses the finite element method to compute elastic responses (Haines *et al.*, 2015; Haines and Wallace, 2020), whereas the body force method adopts analytical expressions for the body force responses (e.g., Sandwell and Wessel, 2016) and uses a Bayesian approach to estimate the strength of forces. Figure 7 illustrates the weighted mean of the four geodetically derived strain rate maps. The mean maximum shear strain rate is similar across all the four methods, whereas the spatial distribution of dilatation and strain rate style differs more significantly (for details see J. Maurer *et al.*, unpublished manuscript, 2023, see Data and Resources). The principal features of the strain-rate field are similar to the previous results of Haines and Wallace (2020).

Fault slip-deficit rates. Slip-deficit rates on faults are obtained from the strain rate maps by adopting the commonly held assumption that the majority of the present-day strain-rate field is elastic recoverable deformation due to interseismic coupling across actively slipping faults (e.g., Reid, 1910). For the geodetic deformation model component of the NZ NSHM 2022, the same faults (and fault geometries) as were used in the geologic deformation model (amended from the gray-colored fault planes in Fig. 1) are discretized into rectangular slip patches, and slip-deficit rates on those patches are estimated by inverting the strain rate maps using the solution in Okada (1992) for surface strain due to uniform slip on a rectangular dislocation in an elastic half-space (Fig. 8). These inversions are detailed in Johnson *et al.* (2022) and K. M. Johnson *et al.*, (unpublished manuscript, 2023 see Data and Resources) and form the basis of the NZ NSHM 2022 geodetic deformation model. Strictly speaking, the NZ NSHM 2022 geodetic deformation model comprises the derived slip-deficit rates on the prescribed upper plate faults.

Four different slip inversion approaches were used for each of the four strain rate maps, each with varying degrees of constraint on the slip-deficit rates from geologic slip rate priors (Johnson *et al.* 2022) and K. M. Johnson *et al.*, (unpublished manuscript, 2023 see Data and Resources). The first approach implements a uniform prior on slip-deficit rate (no preferred rate), with a lower bound of zero (to prevent backward slip) and an upper bound equal to 10 times the geologic deformation model slip rate. This is termed the "No Geologic Prior" inversion because

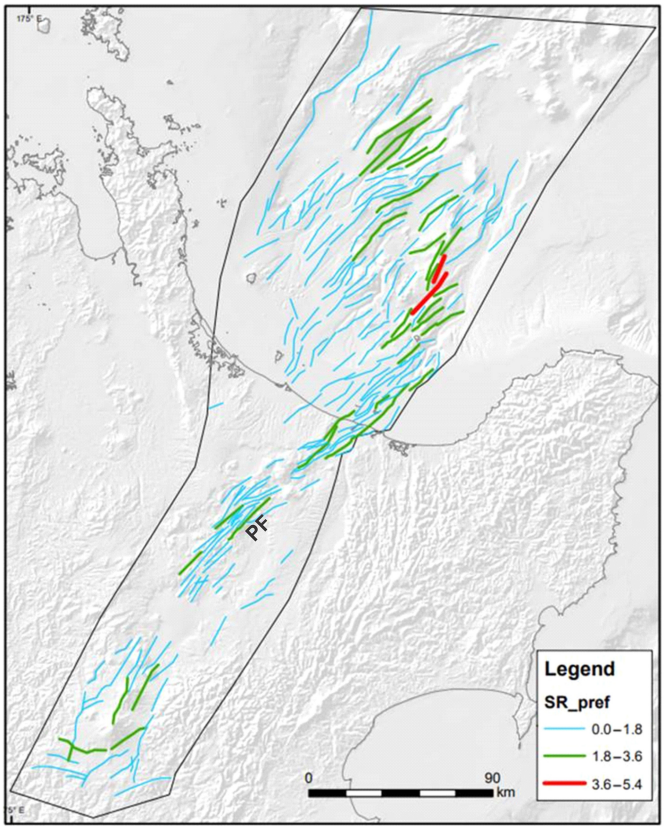

Figure 3. Faults and fault sections in the NZ CFM v.1.0 within the Taupō rift–Havre trough region, color coded by preferred slip rate. Only faults in the Taupō rift–Havre trough region with slip rates ≥ 1.8 mm/yr (depicted as green and red lines) are included in the New Zealand National Seismic Hazard Model (NZ NSHM) 2022 geologic deformation model. PF, Paeroa fault (see also Fig. 4); SR, slip rate in mm/yr. The color version of this figure is available only in the electronic edition.

geologic constraints are only used very loosely. The second approach assumes a truncated Gaussian prior distribution based on the geologic deformation model and is called the "Geologic Prior" inversion. The "No Geologic Prior" and "Geologic Prior" slip-deficit rate inversions reproduce 70%–80% of the total strain-rate field; the remaining 20%–30% cannot be mapped to slip-deficit rates on modeled faults. The other two inversions, with stronger influence from the geologic slip rate priors (such as requiring the slip-deficit rate to be the same as the mean geologic slip rate), fit only 40%–70% of the strain-rate field and were excluded from further consideration.

Ultimately, the "No Geologic Prior" inversion was chosen for use as the single geodetic deformation model in the NZ NSHM 2022. In hazard sensitivity tests, it was found that there was no appreciable difference in ground-shaking hazard throughout the country between the "No Geologic Prior" or the "Geologic Prior" inversion (Gerstenberger, Van Dissen, *et al.*, 2022; M. C. Gerstenberger *et al.*, unpublished manuscript, 2023, see Data and Resources). As geologic slip rates are already incorporated into the NZ NSHM 2022 through the geologic deformation model, using the "No Geologic Prior" inversion spans the largest range of defendable epistemic uncertainty on fault slip rate (slip-deficit rate) in terms of the differences between geology-based and geodesy-based rates.

In final development of the geodetic deformation model (Fig. 8), it was acknowledged that onshore geodetic data provide poor constraints on slip-deficit rates on offshore upper plate faults, and so the geologic deformation model slip rates were assigned as the geodetic model rates for these faults.

SUBDUCTION INTERFACE DEFORMATION MODELS

There are two subduction zones that contribute to ground-shaking hazard in New Zealand: the Hikurangi–Kermadec subduction zone east and northeast of the North Island, where the Pacific Plate is being subducted westward under the Australian plate (Figs. 1, 9); and the Puysegur subduction zone in the southwest, where the Australian plate is being obliquely subducted northeastward beneath the Pacific plate along the Puysegur trench (Figs. 1, 10). The deformation models for these two interfaces are summarized subsequently.

Hikurangi–Kermadec subduction interface deformation model

Both the geometry and slip rates (slip-deficit rates) for the Hikurangi–Kermadec subduction interface deformation model in the NZ NSHM 2022 are blends of data, constraints, and interpretations that are available for the Hikurangi portion of the interface, and different data, constraints, and interpretations that are available for the Kermadec portion of the interface.

Geometry. The geometry of the Hikurangi–Kermadec interface deformation model is a blend of the Hikurangi interface geometry of Williams *et al.* (2013) and the Slab2.0 Kermadec interface geometry of Hayes *et al.* (2018). The two are conjoined several hundred kilometers northeast of the North Island through a smooth linear blend. The Hikurangi portion is truncated to the south along the east–west-oriented base of the Chatham Rise—an impinging continental fragment that likely represents the southern termination of Hikurangi subduction (Wallace *et al.*, 2012, and references therein). The northern extent of the Kermadec interface model is taken as the intersection of the trench with the prominent Louisville Seamount Chain (Fig. 9). This location was chosen, because prominent structural features on the incoming plate are thought to act as barriers to interface ruptures (e.g., Philibosian and Meltzner, 2020). Although such barriers are not always persistent, we feel that this transition is a plausible (and conservative) location to use as the northernmost likely extent of a hypothetical joint Hikurangi–Kermadec rupture. We note that the Hikurangi–Kermadec interface model has an along-strike length of ~2200 km, which is almost double the ~1300 km length of the 2004 Sumatra earthquake—the longest known earthquake

Figure 4. Oblique aerial view looking southwest along the strike of the Paeroa fault, Taupō rift. See Figure 3 for location. GNS Science visual medial library photo ID number is 129653. The color version of this figure is available only in the electronic edition.

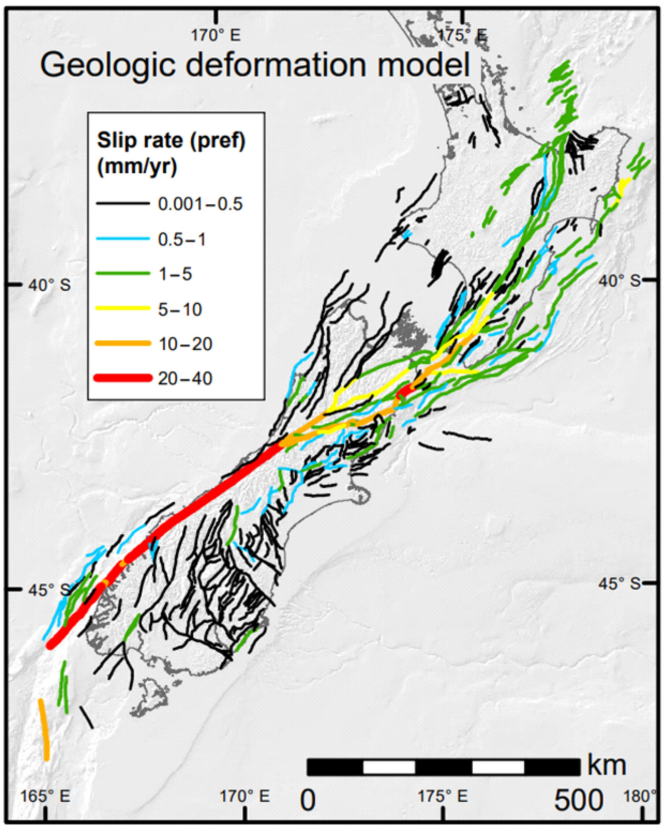

Figure 5. Map view of the NZ NSHM 2022 geological deformation model, with fault traces color coded by preferred slip rate. The color version of this figure is available only in the electronic edition.

rupture (e.g., Ammon *et al.*, 2005). Although we cannot rule out the possibility of a large event breaking across the Louisville Seamount Chain, such an event would only be worth including in the NZ NSHM 2022 if it also extended far south enough to pose a ground-shaking hazard to New Zealand. This, by definition, would mean it would be even be longer than those considered here and be even further outside historic precedent or constraints from other earthquakes.

The Hikurangi–Kermadec interface geometry extends to a depth of 60–70 km, which, at least along the southern Hikurangi interface, marks the approximate down-dip extent of deep slow-slip events (Wallace, 2020).

Slip-deficit rate: Hikurangi. Slip-deficit rates on the Hikurangi portion of the Hikurangi–Kermadec deformation model are derived using the block modeling methods described in Wallace *et al.* (2004, 2012), in which geological fault slip rates (representing relative rates of motion between tectonic blocks) and the interseismic geodetic velocity field are jointly inverted to solve for poles of rotation of discrete tectonic blocks and the degree of interseismic coupling on block-bounding faults (including the subduction interface). For the NZ NSHM 2022, updates were made to the Hikurangi model of Wallace *et al.* (2012), as detailed in Johnson *et al.* (2022). The main updates include: (a) incorporation of the revised Hikurangi interface geometry of Williams *et al.* (2013); (b) incorporation of not only horizontal GNSS velocities but also vertical deformation rates from Interferometric Synthetic Aperture Radar and continuously operating GeoNet GNSS sites (e.g. Hamling, Wright, *et al.*, 2022); (c) incorporation of realistic elastic properties in the deformation model, including observed strong elastic contrasts between the underlying slab and overriding forearc (e.g., Williams and Wallace, 2015); and (d) relaxation of assumptions made in the previous inversions (Wallace *et al.*, 2004, 2012) that forced a monotonic down-dip decrease in interseismic coupling.

For the purposes of the NZ NSHM 2022, we modify the newly developed slip-deficit rate model to also allow for the possibility of rupture within the area where slow-slip

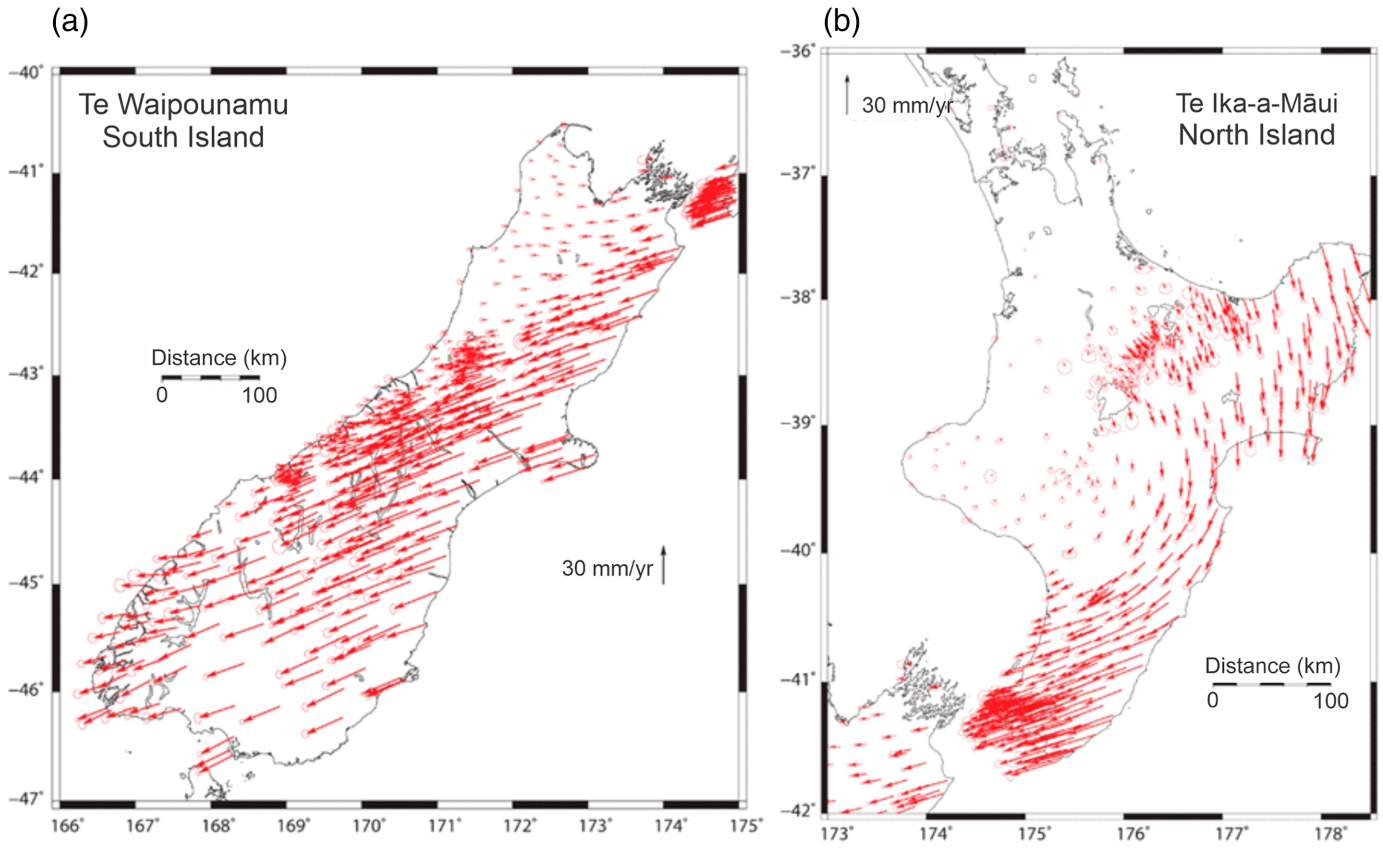

Figure 6. Global Navigation Satellite Systems (GNSS) velocity field from Beavan *et al.* (2016), relative to a fixed Australian plate. (a) South Island and (b) North Island. The color version of this figure is available only in the electronic edition.

events are currently observed (e.g., Wallace, 2020) by manually increasing the slip-deficit rates in these locations. There is also paleoseismic evidence for possible rupture of the subduction interface offshore the central Hikurangi margin in great earthquakes (e.g., Clark *et al.*, 2019), in an area where current deformation is dominated by a mixture of slow-slip events and aseismic creep. We increase the slip-deficit rates on the interface in this area to be 20% of the long-term convergence rate, which is consistent with M_w 8 subduction ruptures approximately every 800–1000 yr. The modified slip-deficit rate models used in the NZ NSHM 2022 are shown in Figure 11.

As noted in Wallace *et al.* (2012), and in Johnson *et al.* (2022), the block-model-based slip-deficit rate results for the Hikurangi interface are based on onshore geodetic data and therefore have little resolution in the offshore regions of the subduction interface. Therefore, we develop two deformation models for the Hikurangi subduction zone: one that is locked to the trench, termed the "locked to trench" rendition (Fig. 11a), and a second model that has much smaller slip-deficit rates offshore termed the "creeping at trench" rendition (Fig. 11b). The first model allows for seismic rupture to the trench and also within the shallow slow-slip event source region, whereas the second model allows for the possibility of minimal seismic rupture on the offshore plate boundary; together these two models allow us to explore the epistemic uncertainty related to offshore interface earthquake rupture, which is not currently well understood. For additional details regarding the derivation of these two Hikurangi slip-deficit rate models, see Van Dissen *et al.* (2022).

Slip-deficit rate: Kermadec. Derivation of slip-deficit rate for the Kermadec portion of the Hikurangi–Kermadec deformation model is based on convergence rate and locking (coupling coefficient) considerations.

Convergence rate along the Kermadec interface is taken from Power *et al.* (2012), who used constraints on elastic block models afforded by Pacific plate-Australian plate (PAC-AUS) motion, Raoul Island GPS velocities, earthquake slip vectors on the interface, and transform orientations in the Havre trough. There is a significant northward increase in convergence rate from ~50 to 85 mm/yr, largely as a result of a northward increase in PAC-AUS relative motion. Back-arc rifting in the Havre trough (and trenchward motion of the Kermadec Arc relative to the Australian plate) also means that the actual convergence rate at the trench is higher than the PAC-AUS relative plate rate, which is accounted for in the block modeling and convergence rate calculations.

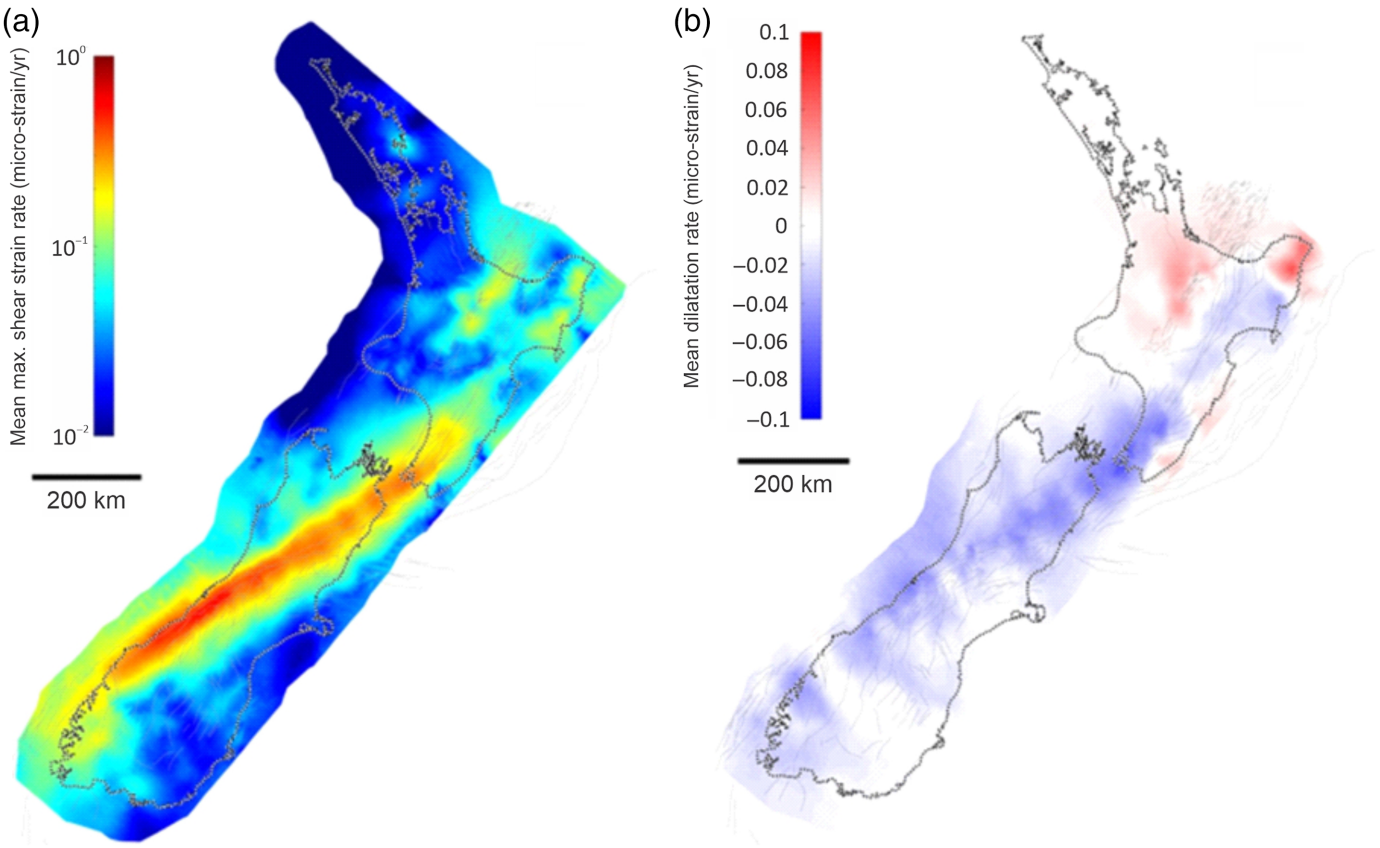

Figure 7. Weighted mean of (a) maximum shear strain rate and (b) dilatation rate of the four strain rate methods employed in the NZ NSHM 2022 geodetic deformation model. Weighting is based on the derived uncertainties of each method. See J. Maurer *et al.* (unpublished manuscript, 2023, see Data and Resources) for details regarding the derivation of these maps as well as those derived for the four individual strain rate methods. The color version of this figure is available only in the electronic edition.

Because of the largely submarine nature of the Kermadec forearc, there are no constraints from geodetic measurements on interseismic coupling (slip-deficit) accumulation on the Kermadec subduction interface, except from Raoul Island, where GPS velocities suggest that the plate boundary is locally strongly locked down to at least 40 km depth (Power *et al.*, 2012). For the remainder of the Kermadec trench region, observed changes in earthquake density along the margin (Bassett *et al.*, 2016) are used to inform variations in coupling coefficient. These along-margin changes in earthquake density also correlate with large changes in overriding plate properties, which may be strongly influencing seismic slip behavior there (Bassett *et al.*, 2016). The NZ NSHM 2022 uses an interface coupling coefficient of 0.2 south of 32.5° S (for which Bassett *et al.*, 2016, postulate a largely creeping interface), a coupling coefficient of 0.5 north of 31° S (also encompassing the Raoul Island area, where higher coupling is observed geodetically), and a linearly increasing transition zone from 0.2 coupling to 0.5 coupling between 32.5° S and 31° S.

Slip-deficit rate: Hikurangi and Kermadec combined. The two Hikurangi slip-deficit rate renditions ("locked to trench" and "creeping at trench") are smoothly combined with the single Kermadec slip deficit model to yield two alternate slip-deficit rate characterizations for the Hikurangi–Kermadec interface. Figure 12 shows these two alternate models. In hazard sensitivity tests undertaken by Gerstenberger, Van Dissen, *et al.* (2022), M. C. Gerstenberger *et al.* (unpublished manuscript, 2023, see Data and Resources), there was no appreciable difference in ground-shaking hazard throughout the country between the two renditions. For reasons of computation efficiency, a single model—the "locked to trench" version—was chosen for use in the final NZ NSHM 2022.

In the NZ NSHM 2022, the Hikurangi–Kermadec subduction interface deformation model surface is discretized into adjoining 30 km × 30 km quadrilateral patches. In the supplemental material, as a csv file, the longitude, latitude, and depth of the upper two corners of each tile of the "locked to trench" rendition are provided (noting that the upper two corners share the same depth). Also provided for each tile are slip rate (slip-deficit rate) in mm/yr, dip angle in degrees, and lower depth (in km below sea level). However, rake is not explicitly specified for the tiles that comprise the interface deformation model, but it is assumed to be predominantly reverse dip-slip for subsequent ground-motion characterization (Bradley *et al.* 2022; B. A. Bradley *et al.*, unpublished manuscript, 2023, see Data and Resources).

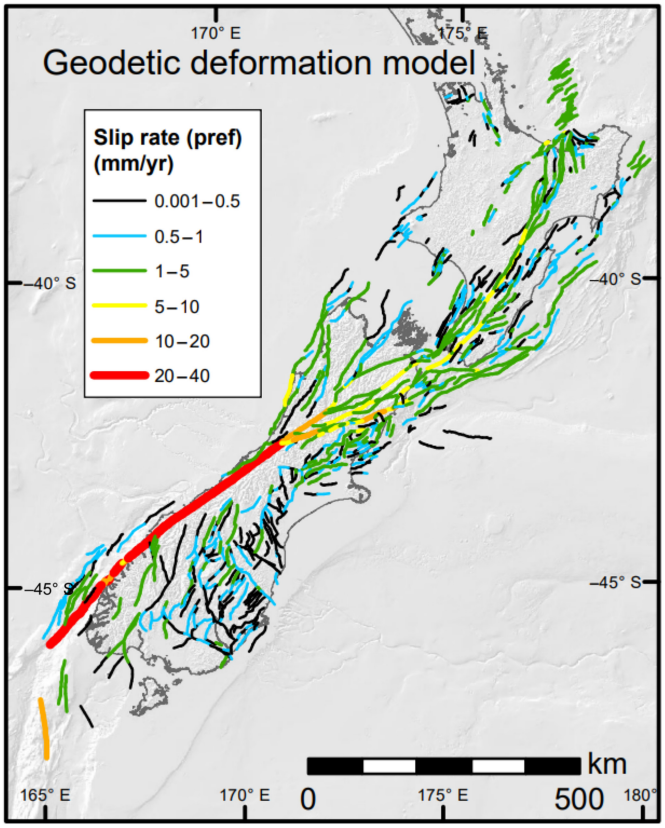

Figure 8. Map view of the NZ NSHM 2022 geodetic deformation model with fault traces color coded by preferred depth-averaged slip-deficit rate. The rates depicted here are the median of the four best-fitting "No Geologic Prior" inversions (one inversion for each strain rate map with minimal geologic slip rate prior). Also, as depicted here, and as comprises the final geodetic deformation model used in the NZ NSHM 2022, the geodetically unconstrained slip-deficit rates for offshore faults have been replaced with the geologic deformation model slip rates. After Johnson *et al.* (2022) and K. M. Johnson *et al.*, (unpublished manuscript, 2023 see Data and Resources). The color version of this figure is available only in the electronic edition.

Slip-deficit rate roughening of the Hikurangi–Kermadec subduction interface deformation models. Initial earthquake rupture rate inversions of the Hikurangi–Kermadec subduction interface deformation models resulted in unrealistic concentrations of $M_w < 8$ earthquake occurrence at specific locations along the edges of the models, rather than being more evenly distributed across the length and breadth of the interface. This was a consequence of the rather smooth and in places homogeneous slip-deficit rate distribution across the interface (Fig. 12), and the rectangular shape and uniform coseismic slip distribution ascribed to the ruptures in the rupture set. Basically, when ruptures are allowed to be large compared to the total fault size (say two-third of it), and the ruptures can be located anywhere on the fault, the ends of the fault will only be involved in ruptures that go all the way to the ends, whereas the center will be involved in all of the large ruptures. So, these larger ruptures both preferentially accommodate more of the slip rate from the center and leave slip rate at the ends that needs to be taken-up by smaller ruptures. To prevent this artificial "edge effect" and to distribute the occurrence of $M_w < 8$ earthquakes more evenly across the interface, we undertook a systematic roughening of the deformation models' slip-deficit rate distribution through a correlated noise approach. The specific recipe for this slip-deficit rate roughening is presented in the Appendix. In summary, each patch on the interface is the center of one perturbation, with a radius drawn from an inverse exponential distribution, and all of the patches in that radius have their slip-deficit rates perturbed by a number drawn randomly from a Gaussian distribution with sigma equal to 15% of their individual slip-deficit rates (such that if the random number were exactly 1, all patches in the radius would have exactly 15% added to their slip-deficit rates). Then, to ensure that the roughened slip models collectively average out to the original deformation model slip-deficit rates, a "mirror" of each perturbed slip model is created and used as well, in which all the perturbations are sign-flipped (Fig. 13). A mean rupture rate model was then constructed from the inversions of several noise realizations (Gerstenberger, Van Dissen, *et al.*, 2022; M. C. Gerstenberger *et al.*, unpublished manuscript, 2023, see Data and Resources).

Puysegur subduction interface deformation model

Geometry. The geometry of the Puysegur subduction interface is taken directly from the NZ CFM v.1.0 (Seebeck *et al.*, 2022, 2023). That said, there is considerable uncertainty about whether the Alpine fault truncates the up-dip portion of the Puysegur interface or whether it soles out onto the interface. To acknowledge this uncertainty, the NZ CFM v.1.0 presents two renditions of the Puysegur interface geometry—one that is truncated by the Alpine fault (Fig. 14) and one that is not (see Seebeck *et al.*, 2022 for more detail). For the NZ NSHM 2022, the first rendition was chosen. This representation mimics the "ploughshare" geometry of Reyners *et al.* (2002) has similarities to the previous interpretations such as Hayes and Furlong (2010) and adopts the Lebrun *et al.* (2000) interpretation in which the up-dip portion of the Puysegur interface is truncated by the Alpine fault.

Slip-deficit rate. The slip-deficit rate applied to the Puysegur subduction interface in the NZ NSHM 2022 is derived from plate convergence rate and interface coupling considerations. The convergence rate is based on the AUS-PAC Euler pole of rotation presented in Wallace *et al.* (2007), and a coupling coefficient of 0.7 is adopted based on the Global Earthquake Model coupling coefficient listed in Berryman *et al.* (2015) (which was based on interseismic coupling models of the Puysegur trench from Wallace *et al.*, 2007). This yields a slip-deficit rate on most of the interface of ~27 mm/yr (Fig. 14).

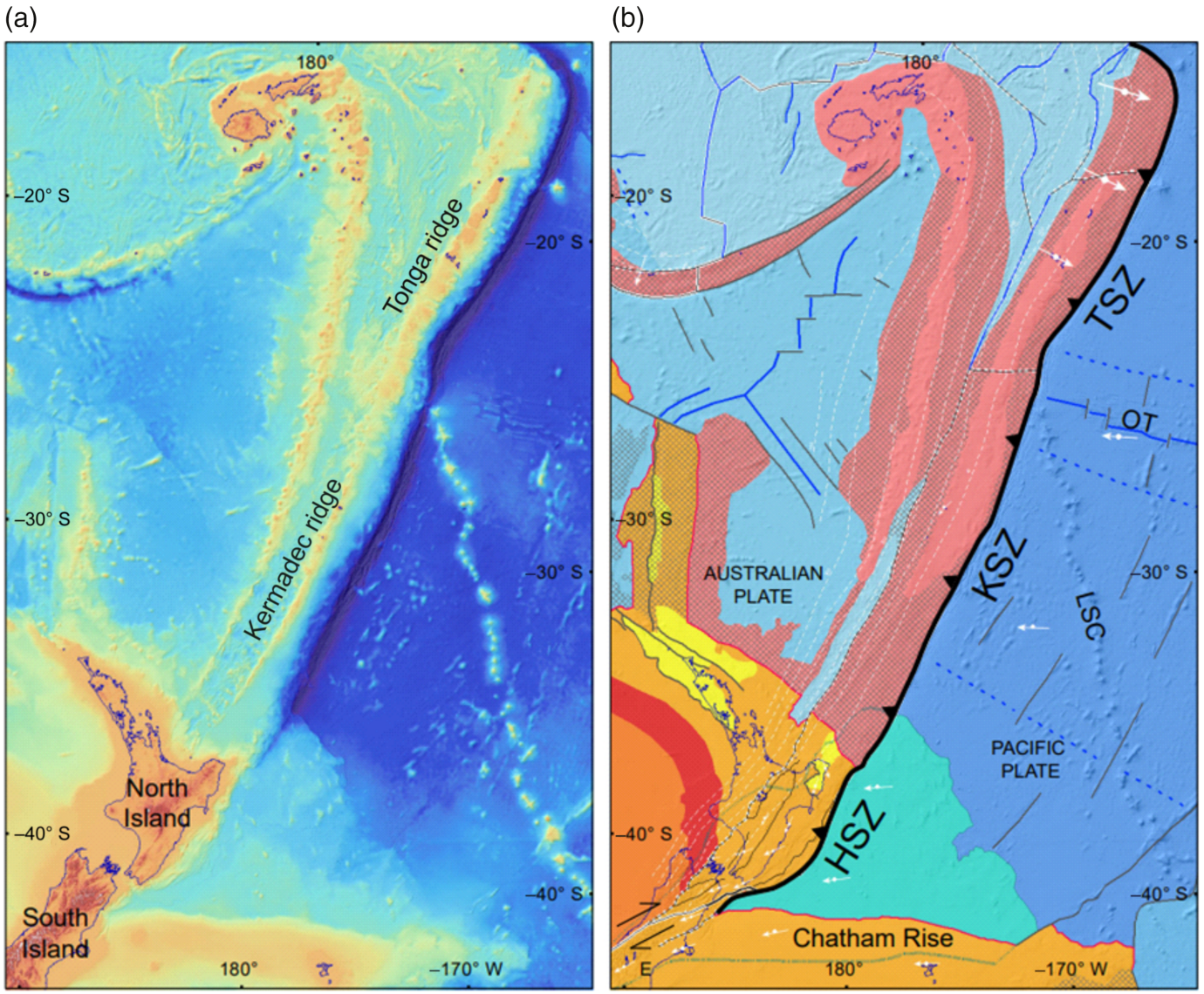

Figure 9. (a) Bathymetric and (b) tectonic maps of the Hikurangi–Kermadec region of Zealandia (from Mortimer *et al.*, 2020). On the tectonic map, blue and green colors denote oceanic crust, orange and yellow colors denote continental crust, and dark pink denotes volcanic arc. HSZ, Hikurangi subduction zone; KSZ, Kermadec subduction zone; LSC, Louisville Seamount chain; OT, Osbourn trough; and TSZ, Tonga subduction zone. The color version of this figure is available only in the electronic edition.

For use in the inversion models, the Puysegur interface is discretized into 15 km × 15 km patches, smaller than the 30 km × 30 km patches used in the Hikurangi–Kermadec discretization. The Puysegur interface is much smaller than the Hikurangi–Kermadec interface (only about 15% of the size), and a smaller tile size was needed to accurately represent its geometry. In the supplemental material provided, the longitude, latitude, and depth of the upper two corners of each tile are provided along with slip-deficit rate, dip angle, and lower depth. As with the Hikurangi–Kermadec deformation model, rake is not specified for the tiles that comprise the Puysegur deformation model, but it is assumed to be predominantly reverse dip-slip for subsequent ground-motion characterization.

DISCUSSION

Moment rate comparisons

An indicative comparison of the moment rates derived for each of the NZ NSHM 2022 deformation models is presented in Table 1. The moment rate of the NZ NSHM 2022 is dominated by the subduction interface deformation models, with the Hikurangi–Kermadec interface deformation models having about 8–9 times more moment rate than the upper plate deformation models. Even the moment rate of the much smaller Puysegur interface deformation model exceeds that of the upper plate deformation models (by about 1.6 times) and so too does the moment rate of just the Hikurangi portion of the Hikurangi–Kermadec interface deformation models (by about 1.5–2 times). This is due to the relatively large seismogenic surface area and fast slip rates of the subduction zones. Of the upper plate deformation models, the geodetic

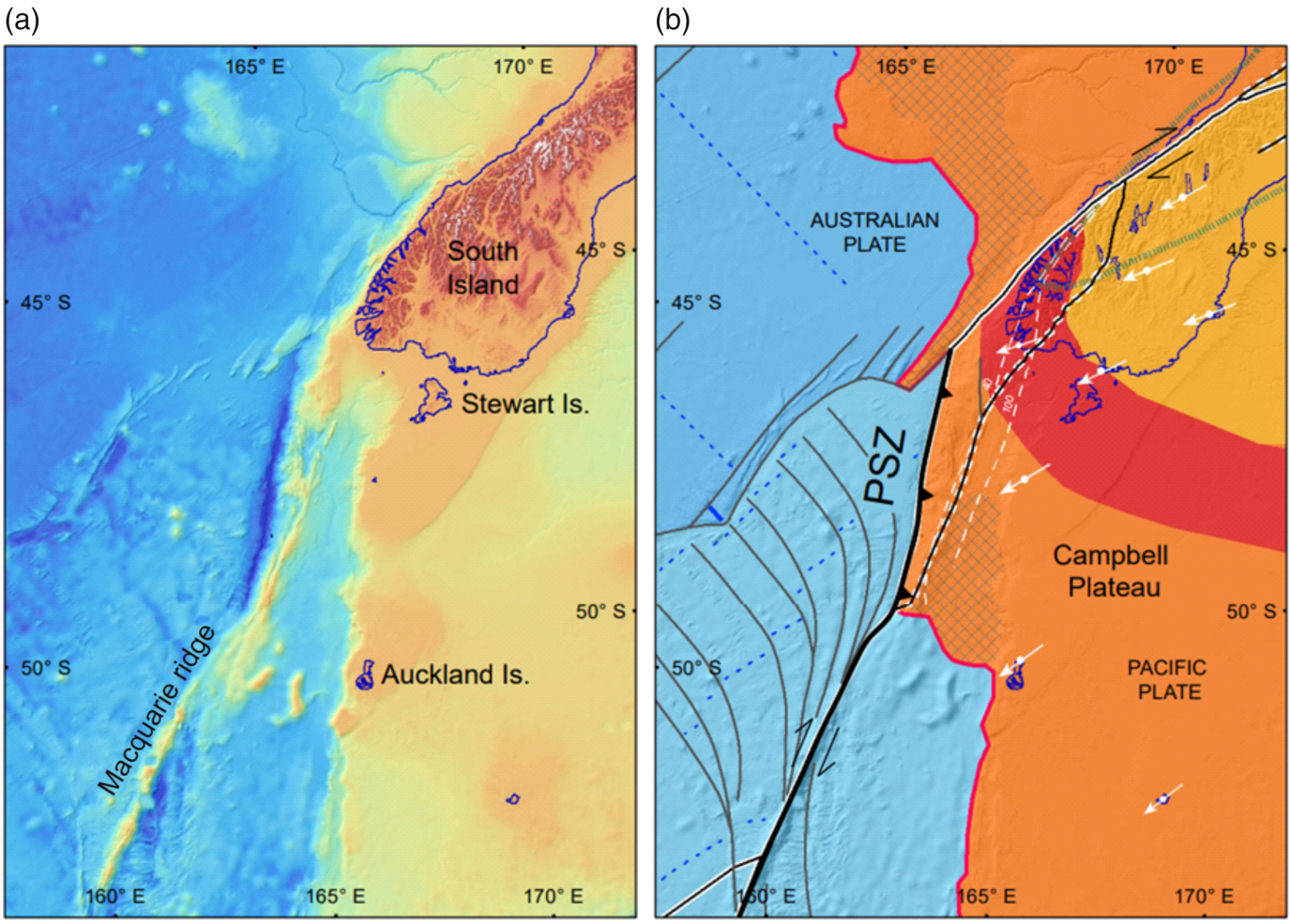

Figure 10. (a) Bathymetric and (b) tectonic maps of the Puysegur subduction zone (PSZ) region of Zealandia (from Mortimer *et al.*, 2020). On the tectonic map, blue colors denote oceanic crust; and orange, red, and yellow colors denote continental crust. The color version of this figure is available only in the electronic edition.

deformation model has slightly more (about 3% more) available moment rate compared to the upper plate geologic deformation model, roughly equivalent to one additional M_w 6 earthquake per year available in the geodetic model compared to the geologic model.

An additional comparison can also be made between the relative amount of "on fault" verses "off fault" deformation in the upper plate geodetic deformation model. In the geodetic deformation model, "on fault" slip-deficit rates account for 70%–80% of the strain-rate field; the remaining 20%–30% is "off fault" or "distributed," with the derivation of "off fault" deformation based on a fit to the residuals remaining after determination of "on fault" deformation (Johnson *et al.*, 2022) and K. M. Johnson *et al.*, (unpublished manuscript, 2023 see Data and Resources). Using the middle (most highly weighted) logic-tree branches of the SRM, ~70% of the total upper plate moment rate is generated "on fault" via the inversion fault model, and ~30% is generated by the distributed seismicity model (K. K. S. Thingbaijam, personal comm., 2023).

Although the coupling coefficients for the Kermadec and Puysegur interfaces are poorly constrained, the deformation models for these interfaces only entertain one set of coupling coefficients. This could be viewed as a distressingly deficient representation of the epistemic uncertainty on the slip-deficit rates on these major faults. But, importantly, the SRM also incorporates logic-tree branches of uniform rupture rate and earthquake rate scaling factors for each of the deformation models (see Gerstenberger, Van Dissen, *et al.*, 2022; M. C. Gerstenberger *et al.*, unpublished manuscript, 2023, see Data and Resources for more detail). The earthquake rate scaling factor (termed "nonstationarity moment rate scaling" in Gerstenberger, Van Dissen, *et al.*, 2022, M. C. Gerstenberger *et al.* (unpublished manuscript, 2023, see Data and Resources) is introduced to account for the possibility of mean earthquake rate variability beyond Poisson (C. Rollins *et al.*, unpublished manuscript, 2023, see Data and Resources). That is, to account for epistemic uncertainty in how representative, or not, the earthquake rate determined from the temporally short instrumental catalog may characterize the actual earthquake rate in the future (in the case of NZ NSHM 2022, over the next

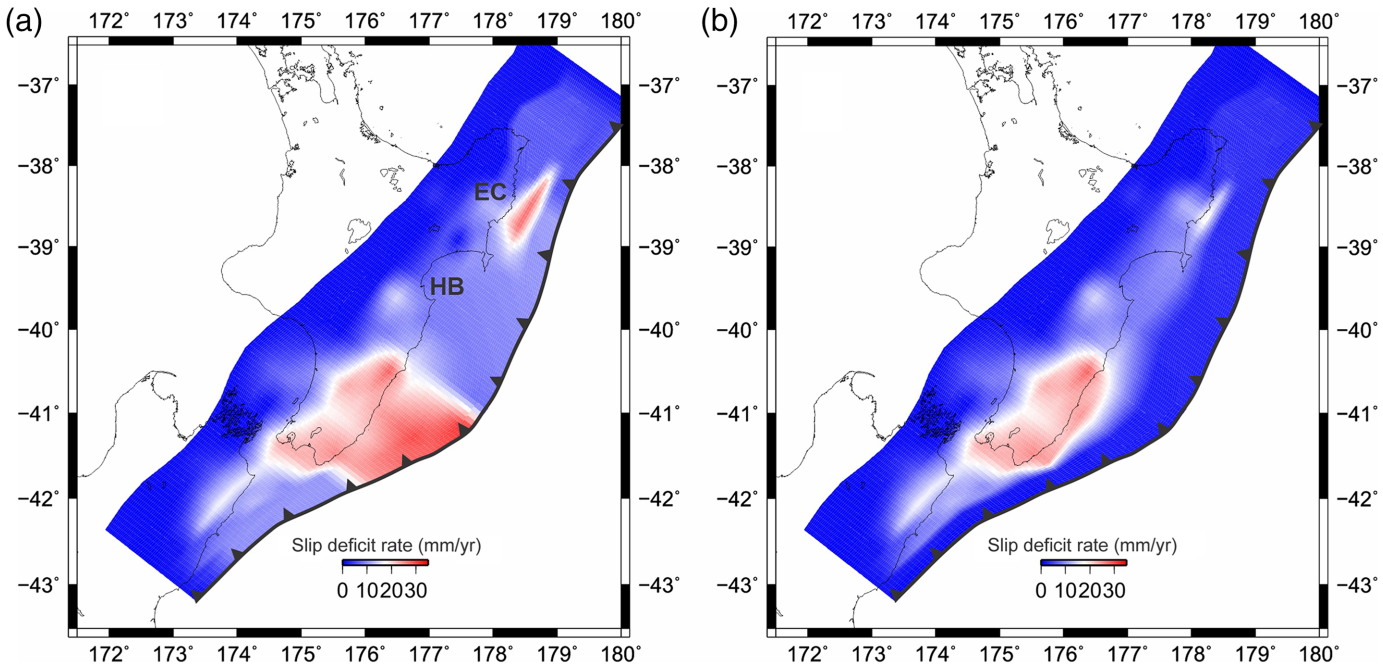

Figure 11. Slip-deficit rate model for the Hikurangi subduction interface developed for the NZ NSHM 2022. Up-dip edge of interface is denoted by toothed black line, with teeth pointing down-dip. A version of this was also used to correct the velocity field for elastic strain due to coupling on the subduction zone prior to inversion of strain rates for upper plate fault slip-deficit rates. (a) "Locked to trench" rendition. EC, East Cape; and HB, Hawkes Bay. (b) "Creeping at trench" rendition. The color version of this figure is available only in the electronic edition.

∼100 yr). In NZ NSHM 2022, the earthquake rate scaling factor is applied to the *N*-value (the number of M_w >5 earthquakes per year) branch of the logic tree and is an important parameter in the inversion-based hazards calculations.

For the Hikurangi–Kermadec subduction interface, the moment rate scaling spans a factor of almost 4, and it spans a factor of ∼6 for the Puysegur interface. These scalings substitute in for deformation model representations of slip-deficit rate epistemic uncertainty on the interfaces.

Slip-deficit rate and slip rate comparisons: geodetic and geologic deformation models. Between the geodetic and geologic deformation models, there are some notable slip rate differences and similarities (Figs. 15, 16). A notable similarity is the onshore portion of the Alpine fault for which geodetic and longer-term geologic rates are quite comparable (see Fig. 16). However, other faults show systematic differences between the rates of the geologic deformation model and the geodetic deformation model, as illustrated in Figure 15. For low-slip-rate faults (i.e., geologic slip rates < ∼1 mm/yr) the geodetic deformation model typical yields higher rates; whereas, the converse is true with the geologic deformation model yielding higher rates for high-slip-rate faults. A consequence of this is that the geodetic deformation model has more moment rate in low-strain-rate regions (compared to the geologic deformation model), and the geologic deformation model has more moment rate in high-strain-rate regions. To further expand on this point, the geologic deformation model encompasses about 360 faults with slip rates ≤ 1 mm/yr (Fig. 5) with the collective available moment rate of these faults being 2.91×10^{18} N · m/yr; whereas, the collective moment rate for the same faults in the geodetic deformation model is 8.15×10^{18} N · m/yr, or about 2.8 times higher (equivalent to about one additional M_w 6.5 earthquake per year). Conversely, the geologic deformation model contains 16 faults with slip rates ≥ 5 mm/yr (these include the Alpine, Hope, Awatere, Wairarapa, and Wellington faults), and the collective moment rate of these 16 high-slip-rate faults is 1.89×10^{19} N · m/yr; whereas, the collective moment rate for the same faults in the geodetic deformation model is 1.50×10^{19} N · m/yr or about 21% lower (equivalent to about one less M_w 6.4 earthquake per year). When summed over the whole upper plate region, these differences mostly cancel out, and the geologic and geodetic models have quite similar total moment rates (Table 1). In addition, and based on sensitivity tests undertaken in the NZ NSHM 2022, hazard runs using the geologic-based models and the geodetic-based models predict similar ground-shaking hazard for cities and towns throughout the country (Gerstenberger, Van Dissen, *et al.*, 2022; M. C. Gerstenberger *et al.*, unpublished manuscript, 2023, see Data and Resources). Important to note here also is that overall hazard in New Zealand is not only dependent just on hazard coming from the upper plate faults but is also dependent other factors such as hazard contributions from the subduction interfaces and the distributed seismicity model. Depending

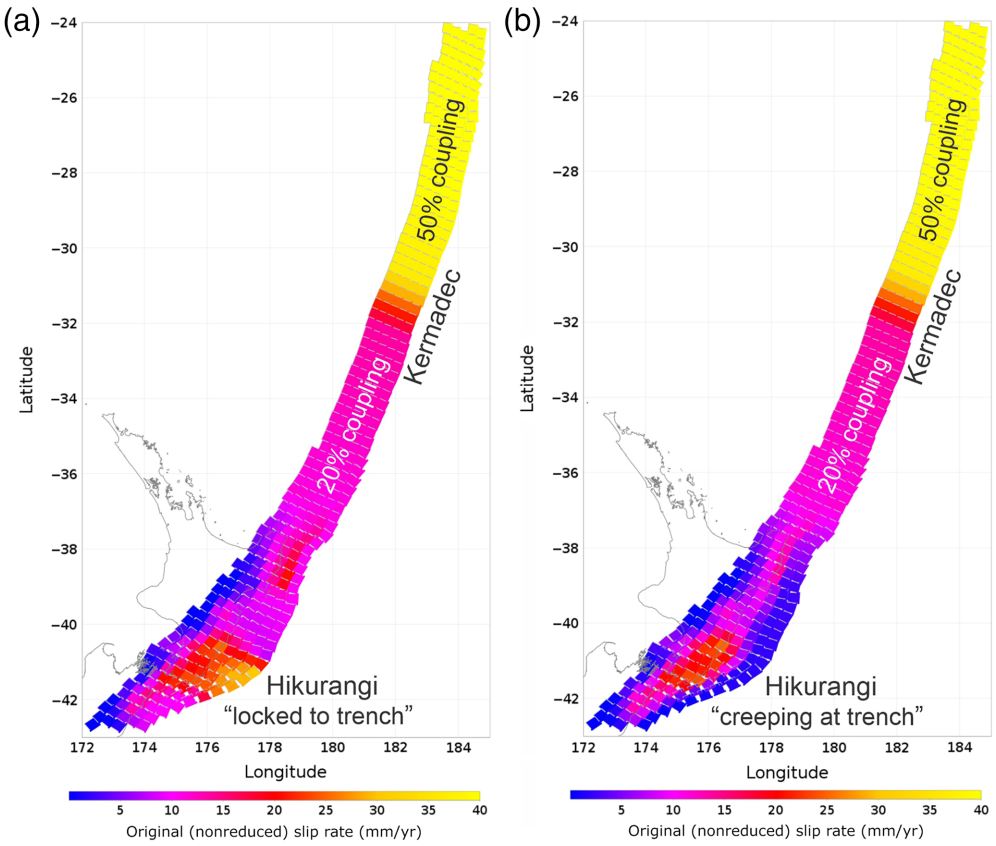

Figure 12. Hikurangi–Kermadec subduction interface deformation models. (a) "Locked to trench" version and (b) "creeping at trench" version. The color version of this figure is available only in the electronic edition.

on location, and the specific hazard probability of exceedance level being considered (e.g., 10% in 50 yr, or 2% in 50 yr), any one of these factors can dominate hazard, and overwhelm

TABLE 1
Deformation Model Moment Rate Comparisons (On-Fault)

Model	Available Moment Rate (N·m/yr)*
Upper plate	
Geologic	2.89×10^{19}
Geodetic (no geologic prior)	2.99×10^{19}
Subduction interface	
Hikurangi–Kermadec†	
Hikurangi (locked to trench) + Kermadec	2.56×10^{20}
Hikurangi (creeping at trench) + Kermadec	2.39×10^{20}
Hikurangi only (locked to trench)	6.22×10^{19}
Hikurangi only (creeping at trench)	4.50×10^{19}
Kermadec only	1.94×10^{20}
Puysegur	4.72×10^{19}

*Available moment rate is the summation of all individual fault moment rates in the specific deformation model for which moment rate = (rigidity) × (fault area) × (fault slip rate), and rigidity is assumed to be 30 GPa.
†–36° latitude marks, approximately, the northern extent of the Hikurangi Plateau and is taken here as the somewhat arbitrary location of the boundary between the northern Hikurangi and southern Kermadec portions of the Hikurangi–Kermadec subduction interface deformation model.

changes and/or differences in the others. In the NZ NSHM 2022, both the upper plate geologic and geodetic deformation models are weighted equally.

Earlier, with regards to various potential geodetic deformation models, we argued that because there was no appreciable difference in ground-shaking hazard predicted using the "No Geologic Prior" inversion compared to the "Geologic Prior" inversion, we considered it satisfactory to use just the "No Geologic Prior" model in the NZ NSHM 2022. It might be argued that because ground-shaking hazard is also not dependent on whether the geologic or geodetic upper plate deformation model is used, that only one of the two need be used. However, the NZ NSHM 2022 will, in future, be interrogated for purposes other than ground-shaking hazard assessment and used on scales smaller than national. In such uses, the local-scale differences between the geologic and geodetic deformation models may be more impactful, and so it would not be appropriate for the NZ NSHM 2022 to choose only one set of slip rates and cut out the other (and much of the epistemic uncertainty along with it).

Differences in rates between geodetic-based and geologic estimates could have several (not mutually exclusive) explanations, such as: (a) ambiguity and trade-offs in deriving fault-specific slip-deficit rates for closely spaced faults (e.g., the closely spaced Hope fault and Clarence fault pair); (b) mismodeling of the geodetic data due to incorrect model fault geometry (e.g., dip of the fault at depth, rake, and number of faults) or Earth structure (e.g., elastic heterogeneity); and (c) inaccurate fault slip rate estimates from geological investigations and/or inferences. Importantly, also, some of these discrepancies might possibly result from time-dependent deformation; the geodetic-based slip-deficit rates and geologic rates capture deformation rates over very different time periods, and the geodetic data may be revealing present-day rates that differ from the longer-term geologic rates in a fashion similar to the large temporal variations in fault slip rate as has been documented over 10^3yr time scales for several major faults throughout New Zealand (e.g., Ninis *et al.*, 2013; Zinke

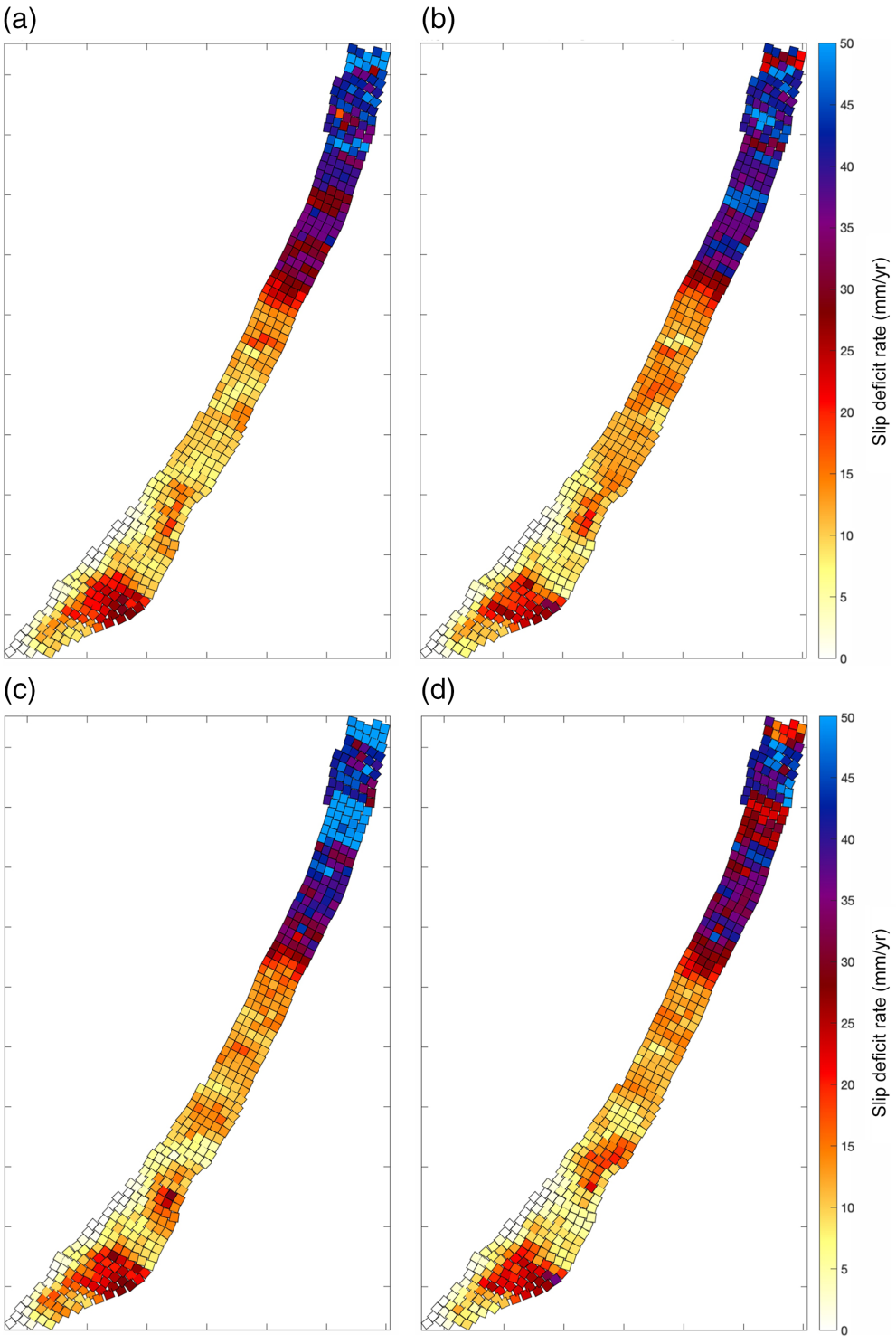

Figure 13. Examples of slip-deficit rate roughened realizations of the (a,c) "locked to trench" Hikurangi–Kermadec subduction interface deformation model and (b,d) corresponding "mirrors." In NZ NSHM 2022, the interface deformation models have an imposed M_{min} of M_w 7.5 and, accordingly, the interface deformation models have had their slip-deficit rates reduced to account for the moment embodied by the "nonoccurrence" of earthquakes ≤ M_w 7.5. The color version of this figure is available only in the electronic edition.

et al., 2017, 2019, 2021; Hatem *et al.*, 2020; Van Dissen *et al.*, 2020). Future versions of the NZ NSHM could potentially explore this by incorporating time-dependent earthquake-cycle deformation or other time varying aspects into their deformation models.

CONCLUSIONS

As part of the NZ NSHM 2022, deformation models were constructed for the upper plate faults and subduction interfaces that impact ground-shaking hazard in the country. These deformation models provide the locations, geometries, and slip rates of the earthquake-producing faults explicitly modeled within the NZ NSHM 2022.

The two subduction zones proximal to New Zealand—the Hikurangi–Kermadec and Puysegur interfaces—comprise the vast majority of overall moment rate in the NZ NSHM 2022 and, accordingly, epistemic uncertainties on their slip-deficit rates are quite relevant to overall hazard. In NZ NSHM 2022, these epistemic uncertainties are largely encompassed in the moment rate scaling of rupture rates in downstream hazard calculations (Gerstenberger, Van Dissen, *et al.*, 2022; M. C. Gerstenberger *et al.*, unpublished manuscript, 2023, see Data and Resources), rather than explicit exploration of slip-deficit rate uncertainly; though the latter was entertained on the Hikurangi portion of the interface through the construction of "locked to trench" and "creeping at trench" slip-deficit rate models. The locking state in the Kermadec portion is less well constrained, and a single slip-deficit rate model is developed based on geodetic plate convergence rates and rheological considerations about locking. This single Kermadec realization is blended with each of the two Hikurangi slip-deficit rate models to yield two overall

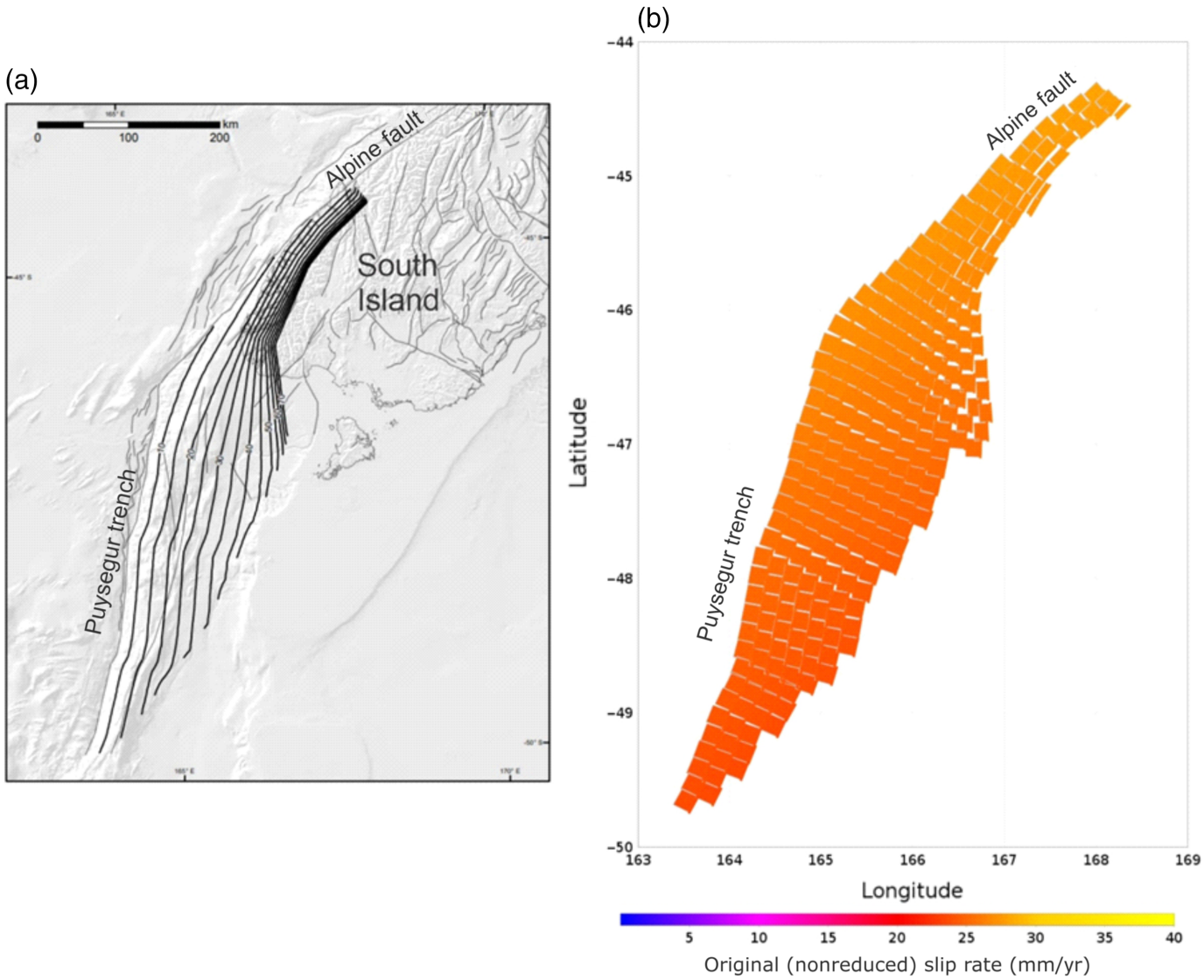

Figure 14. Puysegur subduction interface deformation model. Geometry from Seebeck *et al.* (2022) and slip-deficit rate derived using the Australian plate-Pacific plate (AUS-PAC) Euler pole of rotation of Wallace *et al.* (2007) and the coupling coefficient of 0.7 from Berryman *et al.* (2015). (a) Location with contours on interface geometry in 5 km intervals. (b) Slip rate (slip-deficit rate) depicted via a linear scale. The color version of this figure is available only in the electronic edition.

Hikurangi–Kermadec deformation models. In hazard sensitivity tests undertaken by Gerstenberger, Van Dissen, *et al.* (2022), M. C. Gerstenberger *et al.* (unpublished manuscript, 2023, see Data and Resources), there was no appreciable difference in ground-shaking hazard throughout the country between the "locked to trench" and "creeping at trench" renditions, and the "locked to trench" version was eventually chosen as the single model to use in the final NZ NSHM 2022. The geometry of the Puysegur subduction interface is taken directly from the NZ CFM v.1.0, and the slip-deficit rate is derived from published geodetic plate convergence rates and interface coupling estimates.

For the upper plate faults, two deformation models are developed—one using geologic-based slip rates and the other using geodetic strain-rate-based slip-deficit rates. Both the models utilize the same upper plate fault network, and there are systematic differences in fault slip rates between the two models with the geodetic deformation model yielding higher rates for the slowest slipping faults and, conversely, the geologic deformation model having higher rates for the fastest slipping faults. Nevertheless, despite these differences, both the models yield nearly identical over-all moment rates, and Gerstenberger, Van Dissen, *et al.* (2022), M. C. Gerstenberger *et al.* (unpublished manuscript, 2023, see Data and Resources) not only demonstrate that there is negligible difference in ground-shaking hazard in cities and towns throughout New Zealand resulting from utilization of either of the two models, but also note that determination of overall hazard in New Zealand is not just a consequence of earthquake parametrization of the upper plate faults, but it is

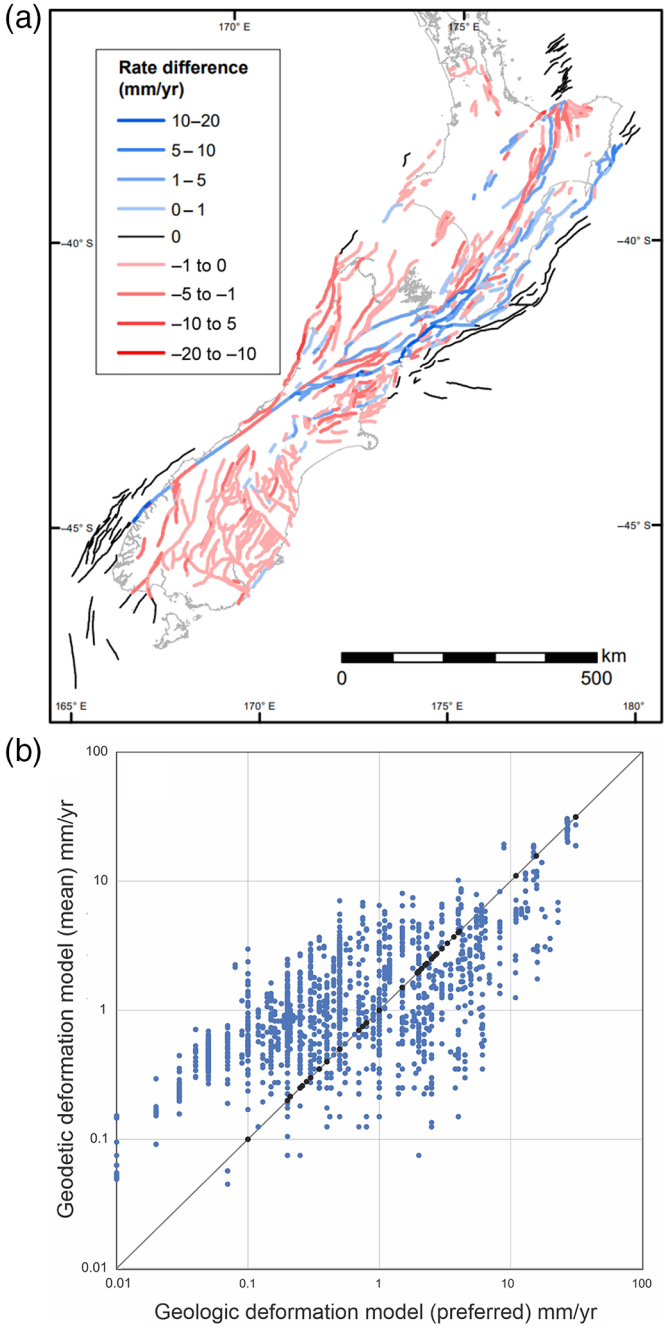

Figure 15. Geological deformation model slip rate and geodetic deformation model slip-deficit rate comparisons. (a) Difference between the preferred geologic slip rates of the geologic deformation model and the mean depth-averaged slip-deficit rates of the geodetic deformation model. Blue colors denote that rates are higher in the geologic deformation model compared to the geodetic model, and red colors denote higher rates in the geodetic deformation model. (b) Comparison of geodetic deformation model depth-averaged slip-deficit rates (vertical axes) and geologic deformation model preferred rates (horizontal axes). Note that the geodetic deformation model used in the NZ NSHM 2022 is based on the "No Geologic Prior" solution and has the poorly constrained slip-deficit rates of the offshore upper plate faults surrounding the country replaced by the geologic deformation model slip rates. The offshore faults in the geodetic deformation model (black dots) that have had their rates replaces by the geologic deformation model rates fall, not surprisingly, on the 1:1 line. The color version of this figure is available only in the electronic edition.

also dependent on other factors such as parametrization of distributed seismicity and the subduction interfaces.

DATA AND RESOURCES

All data used in this article came from published sources listed in the references. The supplemental material contains the following three csv files describing deformation models presented in this article: (1) upper plate geological deformation model: ESup_DFM_1_GeolDefMod_UpperPlate.csv; (2) Hikurangi–Kermadec subduction interface deformation model: ESup_DFM_2_Hik_Kerm_locked_SubInterface.csv; and (3) Puysegur subduction interface deformation model: ESup_DFM_3_Puysegur_SubInterface.csv. Parameters included in the files are described in the Subduction Interface Deformation Models section. The unpublished manuscripts by B. A. Bradley, S. Bora, R. L. Lee, E. F. Manea, M. C. Gerstenberger, P. I. Stafford, G. M. Atkinson, G. Weatherill, J. Hutchinson, C. A. de la Torre, *et al.* (2023), "Ground-motion characterisation models for the 2022 New Zealand National Seismic Hazard Model," submitted to *Bull. Seismol. Soc. Am.*; M. C. Gerstenberger, S. S. Bora, B. A. Bradley, C. DiCaprio, A. Kaiser, E. F. Manea, A. Nicol, C. Rollins, M. W. Stirling, *et al.* (2023), "The 2022 Aotearoa New Zealand National Seismic Hazard Model: Process, overview and results," submitted to *Bull. Seismol. Soc. Am.*; M. C. Gerstenberger, R. J. Van Dissen, C. Rollins, C. DiCaprio, K. K. S. Thingbaijam, S. S. Bora, C. Chamberlain, A. Christophersen, G. L. Coffey, S. M. Ellis, *et al.* (2023), "The seismicity rate model for the 2022 Aotearoa New Zealand National Seismic Hazard Model," submitted to *Bull. Seismol. Soc. Am.*; P. Iturrieta, M. C. Gerstenberger, C. Rollins, R. J. Van Dissen, T. Wang, and D. Schorlemmer (2023), "Least-information uniform rate zone forecasts: Accounting for earthquake rates' temporal and spatial variability," submitted to *Bull. Seismol. Soc. Am.*; J. Maurer, K. Johnson, L. Wallace, I. Hamling, C. Williams, C. Rollins, M. Gerstenberger, and R. Van Dissen (2023), "Geodetic strain rates for the 2022 update of the New Zealand National Seismic Hazard Model," submitted to *Bull. Seismol. Soc. Am.*; S. J. Rastin, D. A. Rhoades, C. Rollins, M. C. Gerstenberger, A. Christophersen, and K. K. S. Thingbaijam (2023), "Spatial distribution of earthquake occurrence for the New Zealand National Seismic Hazard Model revision," submitted to *Bull. Seismol. Soc. Am.*; C. Rollins, , A. Christophersen, K. K. S. Thingbaijam, M. C. Gerstenberger, J. Hutchinson, D. Eberhart-Phillips, S. Bannister, J. Townend, R. Van Dissen, S. J. Rastin, *et al.* (2023), "An integrated earthquake catalogue for Aotearoa New Zealand (version 1) and its implications for earthquake rates: 1. Catalogue assembly, seismological regime classifications, and depth distributions," submitted to *Bull. Seismol. Soc. Am.*; C. Rollins, M. C. Gerstenberger, D. A. Rhoades, S. J. Rastin, A. Christophersen, K. K. S. Thingbaijam, R. J. Van Dissen, T. Wang, J. Fraser, K. Graham, *et al.* (2023), "An integrated earthquake catalogue for Aotearoa New Zealand (version 1) and its implications for earthquake rates: 2. Magnitude-frequency distributions," submitted to *Bull. Seismol. Soc. Am.*; A. Christophersen, S. Bourguignon, D. A. Rhoades, T. I. Allen, J. Salichon, J. Ristau, C. Rollins, M. C. Gerstenberger (2023), "Earthquake magnitude regressions for the 2022 revision of the New Zealand National Seismic Hazard Model," submitted to *Bull. Seismol. Soc. Am.* (This volume - special Issue on Seismic Hazard Modelling); and K. M. Johnson, L. M. Wallace, J. Maurer, I. J. Hamling, C. A. Williams, C. Rollins, M. C.

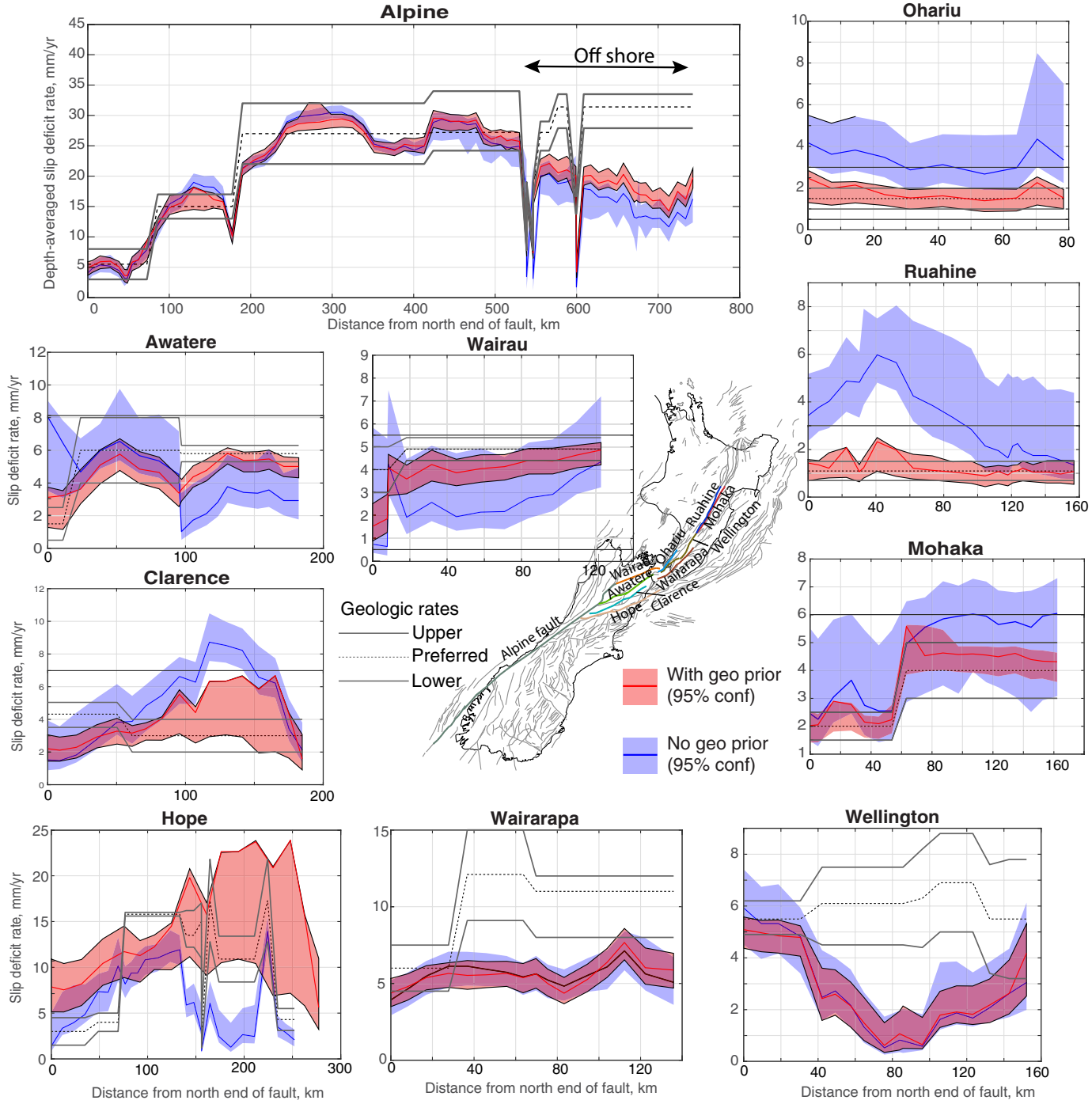

Gerstenberger, R. J. Van Dissen, "Inverting geodetic strain rates for slip deficit rate in complex deforming zones: An application to the New Zealand plate boundary," submitted to *J. Geophys Res.*

DECLARATION OF COMPETING INTERESTS

The authors acknowledge that there are no conflicts of interest recorded.

ACKNOWLEDGMENTS

This work was funded by the New Zealand Ministry of Business, Innovation and Employment to GNS Science via the National Seismic Hazard Revision Project (Contract Number 2020-BD101).

Figure 16. Along-fault depth-averaged "No Geologic Prior" (blue) and "Geologic Prior' (red) slip-deficit rates and comparison with geologic deformation model slip rates. The shading denotes the 95% confidence bounds of the combined (or aggregate) geodetic-based distributions ("No Geologic Prior" and "Geologic Prior") with the solid lines representing the most probable values. As could be expected, the "Geologic Prior" inversion results are shifted closer to the geologic deformation model rates and, in a majority of fault sections, the 95% confidence regions overlap the geologic model rates. However, even with the geologic prior, the estimated slip-deficit rates along sections of the Wairarapa and Wellington faults are lower than the geologic range. After Johnson *et al.* (2022) and K. M. Johnson *et al.*, (unpublished manuscript, 2023 see Data and Resources). The color version of this figure is available only in the electronic edition.

The authors thank the New Zealand National Seismic Hazard Model (NZ NSHM 2022) seismicity rate model (SRM) working group for numerous insightful discussions that gave shape and improved this article. In addition, the authors appreciate the constructive and insightful reviews of early drafts of various aspects of this work by Jessica Murray, John Townend, Ned Field, Nick Horspool, and Marco Pagani, which greatly improved this endeavor. Likewise, the authors wish to acknowledge the reviews of this manuscript by the journal editor and two anonymous reviewers which noticeably improved this paper also.

REFERENCES

Ammon, J. C., C. Ji, H. Thio, D. Robinson, S. Ni, V. Hjorleifsdottir, H. Kanamori, T. Lay, S. Das, D. Helmberger, *et al.* (2005). Rupture process of the 2004 Sumatra-Andaman earthquake, *Science* **308,** 1133–1139.

Bassett, D., H. Kopp, R. Sutherland, S. Henrys, A. B. Watts, C. Timm, M. Scherwath, I. Grevemeyer, and C. E. J. de Ronde (2016). Crustal structure of the Kermadec arc from MANGO seismic refraction profiles, *J. Geophys. Res.* **121,** 7514–7546, doi: 10.1002/2016JB013194.

Beavan, J., L. Wallace, N. Palmer, P. Denys, S. Ellis, N. Fournier, S. Hreinsdottir, C. Pearson, and M. Denham (2016). New Zealand GPS velocity field: 1995-2013, *New Zeal. J. Geol. Geophys.* **59,** 5–14, doi: 10.1080/00288306.2015.1112817.

Berryman, K., L. Wallace, G. Hayes, P. Bird, K. Wang, R. Basili, T. Lay, M. Pagani, R. Stein, T. Sagiya, *et al.* (2015). The GEM faulted earth subduction interface characterisation project, Version 2.0, GEM Foundation, Pavia, Italy, available at http://itic.ioc unesco.org/index.php?option=com_oe&task=viewDocumentRecord&docID=15688 (last accessed May 2022).

Bradley, B. A., S. Bora, R. L. Lee, E. F. Manea, M. C. Gerstenberger, P. I. Stafford, G. M. Atkinson, G. Weatherill, J. Hutchinson, C. A. de la Torre, *et al.* (2022). Summary of the ground-motion characterisation model for the 2022 New Zealand National Seismic Hazard Model, *GNS Science Rept. 2022/46*, GNS Science, Lower Hutt, New Zealand, 44 pp., doi: 10.21420/9BMK-ZK64.

Christophersen, A., S. Bourguignon, D. A. Rhoades, T. I. Allen, J. Salichon, J. Ristau, C. Rollins, and M. C. Gerstenberger (2022). Consistent magnitudes over time for the revision of the New Zealand National Seismic Hazard Model, *GNS Science Rept. 2021/42*, GNS Science, Lower Hutt, New Zealand, 76 pp., doi: 10.21420/A2SN-XM76.

Clark, K., J. Howarth, N. Litchfield, U. Cochran, J. Turnbull, L. Dowling, A. Howell, K. Berryman, and F. Wolfe (2019). Geological evidence for past large earthquakes and tsunamis along the Hikurangi subduction margin, New Zealand, *Mar. Geol.* **412,** 139–172, doi: 10.1016/j.margeo.2019.03.004.

Coffey, G. L., C. Rollins, R. J. Van Dissen, D. A. Rhoades, K. K. S. Thingbaijam, K. J. Clark, M. C. Gerstenberger, N. J. Litchfield, and A. Nicol (2022). New Zealand National Seismic Hazard Model 2022: Earthquake recurrence derivation from paleoseismic data and probability of detection, *GNS Science Rept. 2022/32*, GNS Science, Lower Hutt, New Zealand, 57 pp., doi: 10.21420/2YWK-ZE30.

Coffey, G. L., C. Rollins, R. J. Van Dissen, D. A. Rhoades, K. K. S. Thingbaijam, M. C. Gerstenberger, and N. J. Litchfield (2023). Paleoseismic earthquake recurrence interval derivation for the 2022 revision of the New Zealand National Seismic Hazard Model, *Seismol. Res. Lett.*, doi: 10.1785/0220230197.

Ellis, S., S. Bannister, R. Van Dissen, D. Eberhart-Phillips, C. Holden, C. Boulton, M. Reyners, R. Funnell, N. Mortimer, P. Upton, *et al.* (2023). New Zealand Fault-Rupture Depth Model v1.0: A provisional estimate of the maximum depth of seismic rupture on New Zealand's active faults, *Bull. Seismol. Soc. Am.* doi: 10.1785/0120230166.

Ellis, S. M., S. Bannister, R. J. Van Dissen, D. Eberhart-Phillips, C. Boulton, M. E. Reyners, R. Funnell, N. Mortimer, and P. Upton (2021). New Zealand Fault-Rupture Depth Model v1.0: A provisional estimate of the maximum depth of seismic rupture on New Zealand's active faults, *GNS Science Rept. 2021/08*, GNS Science, Lower Hutt, New Zealand, 47 pp., doi: 10.21420/4Q75-HZ73.

Field, E. H., T. H. Jordan, and C. A. Cornell (2003). OpenSHA: A developing community-modeling environment for seismic hazard analysis, *Seismol. Res. Lett.* **74,** 406–419, doi: 10.1785/gssrl.74.4.406.

Field, E. H., R. J. Arrowsmith, G. P. Biasi, P. Bird, T. E. Dawson, K. R. Felzer, D. D. Jackson, K. M. Johnson, T. H. Jordan, C. Madden, *et al.* (2014). Uniform California earthquake rupture forecast, version 3 (UCERF3)—The time-independent model, *Bull. Seismol. Soc. Am.* **104,** 1122–1180, doi: 10.1785/0120130164.

Gerstenberger, M. C., S. S. Bora, B. A. Bradley, C. DiCaprio, R. J. Van Dissen, G. M. Atkinson, C. Chamberlain, A. Christophersen, K. J. Clark, G. L. Coffey, *et al.* (2022). New Zealand National Seismic Hazard Model 2022 revision: Model, hazard and process overview, *GNS Science Rept. 2022/57*, GNS Science, Lower Hutt, New Zealand, 106 pp., doi: 10.21420/TB83-7X19.

Gerstenberger, M. C., R. J. Van Dissen, C. Rollins, C. DiCaprio, C. Chamberlain, A. Christophersen, G. L. Coffey, S. M. Ellis, P. Iturrieta, K. M. Johnson, *et al.* (2022). The seismicity rate model for the 2022 New Zealand National Seismic Hazard Model, *GNS Science Rept. 2022/47*, GNS Science, Lower Hutt, New Zealand, 156 pp., doi: 10.21420/2EXG-NP48.

Haines, A. J., and L. M. Wallace (2020). New Zealand-wide geodetic strain rates using a physics-based approach, *Geophys. Res. Lett.* **47,** doi: 10.1029/2019GL084606.

Haines, A. J., L. L. Dimitrova, L. M. Wallace, and C. A. Williams (2015). *Enhanced Surface Imaging of Crustal Deformation: Obtaining Tectonic Force Fields Using GPS Data*, P. M. de Paula Garcia (Editor), Springer, New York, SpringerBriefs in Earth Science.

Hamling, I., S. Hreinsdottir, and N. Fournier (2015). The ups and downs of the TVZ: Geodetic observations of deformation around the Taupo Volcanic Zone, New Zealand, *J. Geophys. Res.* **120,** 4667–4679.

Hamling, I. J., G. Kilgour, S. Hreinsdottir, E. Bertrand, and S. Bannister (2022). Estimating the distribution of melt beneath the Okataina Caldera, New Zealand: An integrated approach using geodesy, seismology and magnetotellurics, *J. Volcanol. Geotherm. Res.* **426,** 107549, doi: 10.1016/j.jvolgeores.2022.107549.

Hamling, I. J., T. J. Wright, S. Hreinsdóttir, and L. M. Wallace (2022). A snapshot of New Zealand's dynamic deformation field from Envisat InSAR and GNSS observations between 2003 and 2011, *Geophys. Res. Lett.* **49,** no. 2, e2021GL096465, doi: 10.1029/2021GL096465.

Hatem, A. E., J. F. Dolan, R. W. Zinke, R. M. Langridge, C. P. McGuire, E. J. Rhodes, N. Brown, and R. J. Van Dissen (2020).

Holocene to latest Pleistocene incremental slip rates from the east-central Hope fault (Conway segment) at Hossack Station, Marlborough fault system, South Island, New Zealand: Towards a dated path of earthquake slip along a plate boundary fault, *Geosphere* **16,** 1558–1584, doi: 10.1130/GES02263.1.

Hatem, A. E., N. G. Reitman, R. W. Briggs, R. D. Gold, J. A. Thompson Jobe, and R. J. Burgette (2022). Western U.S. geologic deformation model for use in the U.S. National Seismic Hazard Model 2023, *Seismol. Res. Lett.* **93,** 3053–3067, doi: 10.1785/0220220154.

Hayes, G. P., and K. P. Furlong (2010). Quantifying potential tsunami hazard in the Puysegur subduction zone, south of New Zealand, *Geophys. J. Int.* **183,** 1512–1524, doi: 10.1111/j.1365-246X.2010.04808.x.

Hayes, G. P., G. L. Moore, D. E. Portner, M. Hearne, H. Flamme, M. Furtney, and G. M. Smoczyk (2018). Slab2, a comprehensive subduction zone geometry model, *Science* **362,** 58–61, doi: 10.1126/science.aat4723.

Iturrieta, P., M. C. Gerstenberger, C. Rollins, R. J. Van Dissen, T. Wang, and D. Schorlemmer (2022). Accounting for earthquake rates' temporal and spatial variability through least-information uniform rate zone forecasts, *GNS Science Rept. 2022/14*, GNS Science, Lower Hutt, New Zealand, 50 pp., doi: 10.21420/HYDZ-8W17.

Johnson, K. M., L. M. Wallace, J. Maurer, I. J. Hamling, C. A. Williams, C. Rollins, M. C. Gerstenberger, and R. J. Van Dissen (2022). Geodetic deformation model for the 2022 update of the New Zealand National Seismic Hazard Model, *GNS Science Rept. 2021/37*, GNS Science, Lower Hutt, New Zealand, 62 pp., doi: 10.21420/P93X-8293.

Lebrun, J.-F., G. Lamarche, J.-Y. Collot, and J. Delteil (2000). Abrupt strike-slip fault to subduction transition: The Alpine Fault-Puysegur Trench connection, New Zealand, *Tectonics* **19,** 688–706, doi: 10.1029/2000TC900008.

Litchfield, N. J., J. Humphrey, R. Morgenstern, R. M. Langridge, G. L. Coffey, and R. J. Van Dissen (2022). New Zealand paleoseismic site database: Design and overview of version 1.0, *GNS Science Rept. 2021/52*, 27 pp., doi: 10.21420/VTPT-KB52.

Litchfield, N. J., J. Humphrey, R. Morgenstern, R. M. Langridge, G. L. Coffey, and R. J. Van Dissen (2023). New Zealand paleoseismic site database: Design and overview of version 1.0, *Seismol. Res. Lett.* doi: 10.1785/0220230150.

Mortimer, N., B. Smith Lyttle, and J. Black (2020). Tectonic map of Te Riu-a-Māui/Zealandia, *GNS Science Poster*, GNS Science, Lower Hutt, New Zealand, 8 pp., 1 poster, scale 1:8,500,000, available at https://data.gns.cri.nz/tez/ (last accessed April 2023).

Ninis, D., T. A. Little, R. J. Van Dissen, N. J. Litchfield, E. G. C. Smith, N. Wang, U. Rieser, and C. M. Henderson (2013). Slip rate on the Wellington Fault, New Zealand, during the late quaternary: Evidence for variable slip during the Holocene, *Bull. Seismol. Soc. Am.* **103,** 559–579, doi: 10.1785/0120120162.

Okada, Y. (1992). Internal deformation due to shear and tensile faults in a half-space, *Bull. Seismol. Soc. Am.* **82,** 1018–1040, doi: 10.1785/BSSA0820021018.

Philibosian, B., and A. J. Meltzner (2020). Segmentation and supercycles: A catalog of earthquake rupture patterns from the Sumatran Sunda Megathrust and other well-studied faults worldwide, *Quaternary Sci. Rev.* **241,** 106390, doi: 10.1016/j.quascirev.2020.106390.

Pollitz, F. F., E. L. Evans, E. H. Field, A. E. Hatem, E. H. Hearn, K. Johnson, J. R. Murray, P. M. Powers, Z.-K. Shen, C. Wespestad, *et al.* (2022). Western U.S. deformation models for the 2023 update to the U.S. national seismic hazard model, *Seismol. Res. Lett.* **93,** 3068–3086, doi: 10.1785/0220220143.

Power, W., L. Wallace, X. Wang, and M. Reyners (2012). Tsunami hazard posed to New Zealand by the Kermadec and southern New Hebrides subduction margins; an assessment based on plate boundary kinematics, interseismic coupling, and historical seismicity, *Pure Appl. Geophys.* **169,** 1–36, doi: 10.1007/s00024-011-0299-x.

Rastin, S. J., D. A. Rhoades, C. Rollins, M. C. Gerstenberger, A. Christophersen, and K. K. S. Thingbaijam (2022). Spatial distribution of earthquake occurrence for the New Zealand National Seismic Hazard Model revision, *GNS Science Rept. 2021/51*, GNS Science, Lower Hutt, New Zealand, 65 pp., doi: 10.21420/YKQ8-1C41.

Reid, H. F. (1910). The Mechanics of the Earthquake, The California Earthquake of April 18, 1906, *Report of the State Investigation Commission*, Vol. 2, Carnegie Institution of Washington, Washington, D.C.

Reyners, M., R. Robinson, A. Pancha, and P. McGinty (2002). Stresses and strains in a twisted subduction zone – Fiordland, New Zealand, *Geophys. J. Int.* **148,** 637–648, doi: 10.1046/j.1365-246X.2002.01611.x.

Rollins, C., K. K. S. Thingbaijam, J. Hutchinson, M. C. Gerstenberger, A. Christophersen, D. Eberhart-Phillips, S. J. Rastin, and R. J. Van Dissen (2022). An augmented New Zealand earthquake catalogue, event classifications, and models of the depth distribution of shallow earthquakes in the greater New Zealand region, *GNS Science Rept. 2021/58*, GNS Science, Lower Hutt, New Zealand, 83 pp., doi: 10.21420/XT4Y-WY45.

Sandwell, D. T., and P. Wessel (2016). Interpolation of 2-D vector data using constraints from elasticity, *Geophys. Res. Lett.* **43,** 10,703–710,709, doi: 10.1002/2016GL070340.

Seebeck, H., R. J. Van Dissen, N. J. Litchfield, P. M. Barnes, A. Nicol, R. M. Langridge, D. J. A. Barrell, P. Villamor, S. M. Ellis, M. S. Rattenbury, *et al.* (2022). New Zealand Community Fault Model – version 1.0, *GNS Science Rept. 2021/57*, GNS Science, Lower Hutt, New Zealand, 97 pp., doi: 10.21420/GA7S-BS61.

Seebeck, H., R. Van Dissen, N. Litchfield, P. M. Barnes, A. Nicol, R. Langridge, D. J. A. Barrell, P. Villamor, S. Ellis, M. Rattenbury, *et al.* (2023). The New Zealand Community Fault Model – version 1.0: An improved geological foundation for seismic hazard modelling, *New Zeal. J. Geol. Geophys.* doi: 10.1080/00288306.2023.2181362.

Silva, V., H. Crowley, M. Pagani, D. Monelli, and R. Pinho (2014). Development of the OpenQuake engine, the Global Earthquake Model's open-source software for seismic risk assessment, *Nat. Hazards* **72,** 1409–1427, doi: 10.1007/s11069-013-0618-x.

Thingbaijam, K. K. S., M. C. Gerstenberger, C. Rollins, A. Christophersen, C. A. Williams, J. Ristau, S. J. Rastin, J. Fraser, and R. J. Van Dissen (2022). A seismogenic slab source model for New Zealand, *GNS Science Rept. 2021/50*, GNS Science, Lower Hutt, New Zealand, 31 pp., doi: 10.21420/CDMK-3F30.

Thingbaijam, K. K. S., M. C. Gerstenberger, C. Rollins, R. J. Van Dissen, S. J. Rastin, J. Ristau, C. Williams, A. Christophersen, D. Fitzenz, and M. Pagani (2023). A seismogenic slab source model for Aotearoa New Zealand, *Bull. Seismol. Soc. Am.* doi: 10.1785/0120230080.

Van Dissen, R., E. Abbott, R. Zinke, D. Ninis, J F. Dolan, T. A. Little, E. J. Rhodes, N J. Litchfield, and A. E. Hatem (2020). Slip rate

variations on major strike-slip faults in central New Zealand and potential impacts on hazard estimation, *Proc. of the 2020 New Zealand Society for Earthquake Engineering Annual Technical Conference*, New Zealand Society for Earthquake Engineering, Paper No. 6, 8 pp., available at https://repo.nzsee.org.nz/handle/nzsee/1691 (last accessed April 2023).

Van Dissen, R. J., H. Seebeck, L. M. Wallace, C. Rollins, M. C. Gerstenberger, A. Howell, C. DiCaprio, and C. A. Williams (2022). New Zealand National Seismic Hazard Model 2022: Geologic and subduction interface deformation models, *GNS Science Rept. 2022/31*, GNS Science, Lower Hutt, New Zealand, 23 pp., doi: 10.21420/CEXY-AB93.

Wallace, L. M. (2020). Slow slip events in New Zealand, *Annu. Rev. Earth Planet. Sci.* **48,** 175–203, doi: 10.1146/annurev-earth-071719-055104.

Wallace, L. M., P. Barnes, J. Beavan, R. Van Dissen, N. Litchfield, J. Mountjoy, R. Langridge, G. Lamarche, and N. Pondard (2012). The kinematics of a transition from subduction to strike-slip: An example from the central New Zealand plate boundary, *J. Geophys. Res.* **117,** no. B2, doi: 10.1029/2011jb008640.

Wallace, L. M., J. Beavan, R. McCaffrey, K. Berryman, and P. Denys (2007). Balancing the plate motion budget in the South Island, New Zealand using GPS, geological and seismological data, *Geophys. J. Int.* **168,** 332–352, doi: 10.1111/j.1365-246X.2006.03183.x.

Wallace, L. M., J. Beavan, R. McCaffrey, and D. Darby (2004). Subduction zone coupling and tectonic block rotations in the North Island, New Zealand, *J. Geophys. Res.* **109,** no. B12, doi: 10.1029/2004jb003241.

Wang, H., and T. J. Wright (2012). Satellite geodetic imaging reveals internal deformation of western Tibet, *Geophys. Res. Lett.* **39,** L07303 , doi: 10.1029/2012GL051222.

Weiss, J. R., R. J. Walters, Y. Morishita, T. J. Wright, M. Lazecky, H. Wang, E. Hussain, A. J. Hooper, J. R. Elliott, C. Rollins, *et al.* (2020). High-resolution surface velocities and strain for Anatolia from Sentinel-1 InSAR and GNSS data, *Geophys. Res. Lett.* **47,** e2020GL087376 , doi: 10.1029/2020GL087376.

Williams, C. A., and L. M. Wallace (2015). Effects of material property variations on slip estimates for subduction interface slow-slip events, *Geophys. Res. Lett.* **42,** 1113–1121, doi: 10.1002/2014gl062505.

Williams, C. A., D. Eberhart-Phillips, S. Bannister, D. H. N. Barker, S. Henrys, M. Reyners, and R. Sutherland (2013). Revised interface geometry for the Hikurangi subduction zone, New Zealand, *Seismol. Res. Lett.* **84,** 1066–1073, doi: 10.1785/0220130035.

Zinke, R., J. F. Dolan, E. J. Rhodes, R. Van Dissen, A. E. Hatem, C. P. McGuire, N. D. Brown, and J. R. Grenader (2021). Latest Pleistocene–Holocene incremental slip rate of the Wairau fault: Implications for long-distance and long-term coordination of faulting between North and South Island, New Zealand, *Geochem. Geophys. Geosys.* **22,** 1525–2027, doi: 10.1029/2021GC009656.

Zinke, R., J. F. Dolan, E. J. Rhodes, R. Van Dissen, and C. P. McGuire (2017). Highly variable latest Pleistocene-Holocene incremental slip rates on the Awatere fault at Saxton River, South Island, New Zealand, revealed by Lidar mapping and luminescence dating, *Geophys. Res. Lett.* **44,** 11,301–11,310, doi: 10.1002/2017GL075048.

Zinke, R., J. F. Dolan, E. J. Rhodes, R. Van Dissen, C. P. McGuire, A. E. Hatem, N. D. Brown, and R. L. Langridge (2019). Multi-millennial incremental slip rate variability of the Clarence fault at the Tophouse Road site, Marlborough fault system, New Zealand, *Geophys. Res. Lett.* **46,** 771–725, doi: 10.1029/2018GL080688.

APPENDIX

Recipe for slip-deficit rate roughening of the Hikurangi–Kermadec subduction interface deformation models

Looping across all slip patches comprising a specific interface deformation model, at each patch (patch *i*), the following is done:

1. A random number is drawn from a uniform distribution between 0 and 1. That number is used to compute what radius (in units of patch length) will be assigned to the perturbation of slip-deficit rate (the noise) that is centered on that patch.
   a. The likelihood function for the radius is an inverse exponential distribution, so that larger and larger perturbation radii are inverse-exponentially less and less likely (the original random number has to be quite close to 1 to convert to a large perturbation radius). The specific line of MATLAB (www.mathworks.com/products/matlab, last accessed August 2023) code that does this is:
      - Radius = −log(1 − rand(1,1))/2.
      - This is equivalent to rand(1,1) = 1 − exp(−radius/(½)), except rearranged so that it computes the radius given the random number.
   b. As shown in the equation, this inverse exponential distribution has a characteristic dimension of ½. In units of patch length, this is a characteristic radius of half the length of a patch, or 15 km (so a characteristic diameter of one patch length, or 30 km).
2. This radius is then used to compute an area of the slip rate perturbation in units of number of patches (*N*_patches = pi*radius^2).
3. The closest *N*_patches to the patch (patch *i*) are selected for this to be applied to.
4. All of those patches are perturbed by amounts equal to (their individual input slip-deficit rates) × (a random number drawn from a Gaussian distribution with sigma = 0.15). Therefore, a single perturbation gets applied, but scaled locally by the slip-deficit rate of each of the selected patches.
5. The loop then continues for all the other patches.
6. Then all patches with negative slip rates are set to 0.

Manuscript received 28 May 2023
Published online 3 November 2023